Microporous and Mesoporous Materials 276 (2019) 107–132

Contents lists available at ScienceDirect

Microporous and Mesoporous Materials

journal homepage: www.elsevier.com/locate/micromeso

Advancement in porous adsorbents for post-combustion CO_2 capture

Arindam Modak[a,*], Subhra Jana[a,b,**]

[a] Technical Research Centre, S. N. Bose National Centre for Basic Sciences, Block - JD, Sector-III, Salt Lake, Kolkata, 700 106, India
[b] Department of Chemical, Biological & Macro-Molecular Sciences, S. N. Bose National Centre for Basic Sciences, Block - JD, Sector-III, Salt Lake, Kolkata -700 106, India

ARTICLE INFO

Keywords:
Metal-organic frameworks (MOFs)
Zeolitic imidazolate frameworks (ZIF)
Porous organic polymers (POPs)
Covalent organic frameworks (COFs)
Functional oxides
CO_2 capture

ABSTRACT

One of the foremost environmental concerns of our age is the growing concentration of atmospheric CO_2 owing to the fossil fuel, power plants, chemical processing and deforestation. High CO_2 level in atmosphere induces global warming which is considered as one of the major long lasting problems in the twenty-first century and thus intensive efforts are necessary to curb CO_2 from entering into carbon cycle. To address this issue, several promising porous adsorbents are developed to partially mitigate the global climate problems. With increasing substantial interest on high surface area metal-organic frameworks (MOFs), porous organic polymers (POPs), covalent organic frameworks (COFs) and nanoporous oxides, we believe, they could be promising for carbon capture due to their high porosity, presence of ultra-small pores, structural diversity, high stability and excellent recyclability. This review highlights the recent progresses on MOFs, POPs, COFs and mesoporous oxides as CO_2 adsorbent and illustrates their CO_2 separation selectivity and enthalpy of interaction etc. Finally, we conclude with the viewpoint on the future developments in the context of promising adsorbents for CO_2 capture, followed by its transformation to value added products and the potential drawbacks which are associated with them.

1. Introduction

In 20th century, Goddard Institute for Space Studies (GISS) found that global temperature is increasing every year since 1951 on account of global warming and is continuing to increase in the 21st century because of the release of CO_2 as greenhouse gas [1]. Based on such criteria "The Intergovernmental Panel on Climate Change" (IPCC) declares that this excessive CO_2 emission is markedly related to global climate change and hence could affect global temperature [2]. Currently, the CO_2 level in the atmosphere is ~401 ppm, which is 70% higher than that of 280 ppm during pre-industrial times and is expected to increase ~550 ppm in 2050 [3]. As a result, the human body will start suffering as our respiratory system will be affected from balancing between O_2 uptake and release of much strongly bonded CO_2. Additionally, atmospheric temperature will also increase owing to the imbalance of the equilibrium between incoming and outgoing temperature of the earth. Hence, special care is necessary to diminish CO_2 level in the atmosphere.

To regulate carbon level in the atmosphere, CO_2 capture and storage/sequestration (CCS) as well as CO_2 capture and utilization (CCU) techniques are implemented. In CCS process, physical adsorption, absorption and membrane separation technology are being involved to store CO_2 in adsorbents which later buried in deep underground. During CCS process, captured CO_2 is pressurized to 100 bar or even more and then transported to a storage site, where it is injected and safely trapped in underground reservoir for several thousands of years. Liquid amines, such as monoethanolamine, diethanolamine are traditionally being utilized to store CO_2 through CCS processes [4]. However despite the wide use of such approach, it suffers from major drawbacks, like corrosive nature and volatility of amines, decomposition of the generated salts as well as its expensive regeneration cost [5]. Therefore, the large energy penalty and considerable cost of CCS process are slowing down the exploitation of commercial CCS projects. Here, we have described some outlines in carbon capture techniques as well as several characteristic of promising adsorbents which include selectivity, enthalpy of interaction and recyclability.

1.1. Outlines of carbon capture processes

For the reduction of anthropogenic CO_2 emission, it is quite inevitable to explore cost-effective and scalable techniques. To address this issue, several ways can be adopted: a) pre-combustion capture; b) post-combustion capture and c) oxy-fuel combustion. The separation of each type of process has been shown in an outline sketch, given in

* Corresponding author.
** Corresponding author. Technical Research Centre, S. N. Bose National Centre for Basic Sciences, Block - JD, Sector-III, Salt Lake, Kolkata, 700 106, India.
E-mail addresses: arindam.trc@bose.res.in (A. Modak), subhra.jana@bose.res.in (S. Jana).

https://doi.org/10.1016/j.micromeso.2018.09.018
Received 1 August 2018; Received in revised form 9 September 2018; Accepted 18 September 2018
Available online 20 September 2018
1387-1811/ © 2018 Elsevier Inc. All rights reserved.

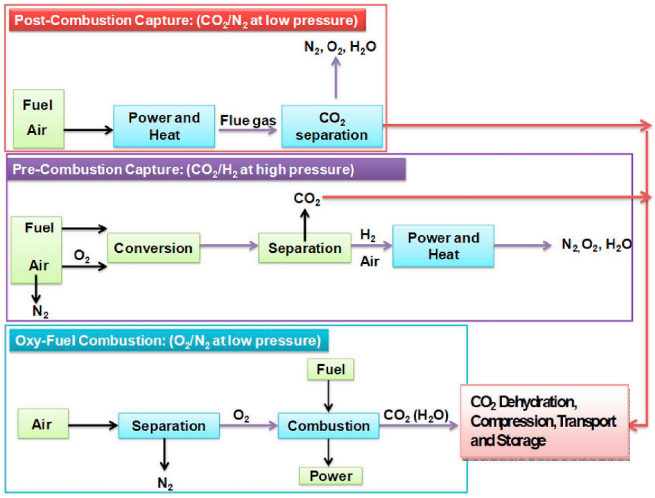

Fig. 1. Schematic representation of different CO_2 capture technologies.

Fig. 1. Additionally, carbon capture for CH_4 purification and direct air capture are also discussed.

1.1.1. Pre-combustion CO_2 capture

The main aim in this process is to separate CO_2 from H_2 at elevated pressures (~30 bar) and temperatures (~40 °C) with an adsorbent bed. Generally fuel reacts with air/O_2 to produce synthesis gas (syn gas), which is composed of a mixture of CO and H_2. Then CO was passed through a swing converter where it reacted with steam, produces CO_2 (25%–35%) and additional H_2 (30%–50%) at high pressure (5–40 bar) in the catalytic reactor. Therefore, pre-combustion technology is associated with the purification of natural gas or syngas (CO + H_2) in order to create suitable feeds regarding energy generation, CO_2 separation, steam reforming process and gasification of coke or oil residues. Recycling of the adsorbents has been done by decreasing pressure. Due to the availability of ~15% CO_2 in the product gas mixture, the separation is quite convenient in this process [6], whereas high temperature of the reactor and H_2-rich turbine fuel cause severe problem.

1.1.2. Post-combustion CO_2 capture

In post-combustion process, CO_2 needs to be separated from N_2 after combustion of fossil fuels, before it enters the atmosphere. Generally, burning of fossil fuel in air generates flue gas, which consists of 15% CO_2, 70% N_2 along with other minor components (H_2O, CO, NO_x, and SO_x) with total pressure of 1 bar and the temperature between 40 and 60 °C. The flue gas later passed through suitable adsorbents for separation of CO_2 and the adsorbed CO_2 after liberated from the sorbent is compressed for transportation and storage. It can be said that the captured CO_2 must have high purity for its compression, transportation and storing underground would be cost-effective. Again after desulfurization, too low concentration of CO_2 (~4% by volume) could be difficult for adsorption; hence efficiency of the adsorbents should be high enough [7].

1.1.3. Oxy-fuel combustion

In the conventional oxy-fuel combustion setup, fossil fuel combustion takes place under nearly pure O_2 atmosphere to reduce the possibility of NO_x generation. During the combustion process, O_2 is fed into the power plant and diluted with CO_2 to a partial pressure of 0.21 bar. The gaseous products from this exhaustion is mainly composed of CO_2 (55%–65%) and H_2O (25%–35%) and if water is successfully removed, nearly pure CO_2 can be directly subjected to sequestration [8]. It is to state that pre-combustion and post-combustion capture can't be easily implanted into industry, whereas 95% of carbon capture processes have been achieved by oxy-fuel combustion process, because of the advantage and simplicity in the separation of flue gas, as it is almost entirely composed of CO_2. However, the implementation of oxy-fuel combustion chamber is challenging and costly due to the rigorous requirement for nearly pure O_2 chamber.

1.1.4. Natural gas purification

For natural gas purification purposes, carbon capture technologies are also being applied. Since, CH_4 is the primary part of natural gas, therefore separation of CO_2 from CH_4 directs topmost research interest. During extraction of natural gas from wells, 20–40 wt% CO_2 is always emitted in the atmosphere. Therefore, purification of natural gas needs special technologies and materials to withstand high pressure during extraction process.

1.1.5. CO_2 capture from ambient air

Among all carbon capture processes, CO_2 capture from ambient air is quite noteworthy and is quite challenging since this strategy deals with CO_2 in highly dilute condition with a partial pressure of ~400 ppm. The successful implementation of this process is seen only in enclosed environments, such as submarines, aircraft etc., however the scope and utility of diverse materials/technologies remains unexplored.

It is pertinent to mention that ever since the discovery of Lackner in 1999, direct extraction of CO_2 from ambient air or direct air capture (DAC) is becoming quite popular as it is applying in real world carbon capture purposes [9]. In addition to the academic research, DAC has been utilized in industrial purposes by engaging with several start-up companies pushing this technology from laboratory scale to pilot level. While conventional CO_2 capture sorbents are mainly focused on point sources, DAC is advantageous since it separates CO_2 from distributed sources as well as point sources. It can be said that post-combustion and DAC are different techniques with different goals, where post-combustion adsorbs CO_2 from exhaust gas and DAC uptakes CO_2 from ambient air. Apart from environmental protection, DAC is advantageous to uphold carbon feedstock, where with the help of this technology anywhere in the globe the adsorbed CO_2 can be utilized to produce fuels, pharmaceuticals or other value-added chemical products [10]. Notably, DAC deals with carbon capture which is nearly 350 times lower than normal coal-based flue gas, therefore under ultra-dilute condition of CO_2, only chemisorbent materials are effective than physisorbent materials, like zeolites, activated carbon, etc. Their performance is inferior at low CO_2 pressure. Till date, very few materials are reported towards DAC [10].

1.2. Enthalpy, selectivity and recyclability during CO_2 adsorption

CO_2 adsorption is a result of interaction between CO_2 and adsorbent, therefore enthalpy of CO_2 adsorption is vital for determining selectivity of CO_2 uptake in presence of other gases. As for example, a material having poor enthalpy of adsorption will show reduced selectivity for CO_2, however the adsorbent have low heat of regeneration energy. Conversely, when CO_2 is strongly bonded with the polar surface, selectivity is high and requires much energy for regeneration. Therefore, it is quite challenging to design materials which can balance the selectivity and low enthalpy for regeneration.

Generally, enthalpy of CO_2 adsorption has been determined from isosteric heat of adsorption (Q_{st}), which is actually the average enthalpy of adsorption for a gas molecule at different binding sites. Q_{st} of CO_2 adsorption can be calculated from CO_2 adsorption isotherms measured at two different temperatures and by fitting the data with a virial-type equation, as shown below [11].

$$lnP = lnN + \frac{1}{T}\sum_{i=0}^{m} a_i N^i + \sum_{j=0}^{n} b_j N^j \quad (1)$$

Where, P is the pressure, N is the absorbed amount of gas, T is

temperature, a_i and b_j are virial coefficients. m and n are the number of virial coefficients required to describe the isotherms. Alternatively, Q_{st} can also be measured using the Clausius–Clapeyron equations [12].

$$\ln P = \frac{-Q_{st}}{RT} + C \tag{2}$$

where, P is pressure, T is the temperature, R is the universal gas constant (8.314 J K^{-1} mol^{-1}), and C is a constant. Generally, Q_{st} decreases with increasing coverage of adsorbate. Therefore at zero coverage, the isosteric heat of adsorption indicates the strongest binding sites in the material and the magnitude of Q_{st} suggests the important features of pore, such as its functionality with amine sites or the presence of open metal sites. It is worth mentioning that CO_2 adsorption proceeds through either physisorption or by chemisorption. Physisorption occurs through weak Van der Waals interactions between adsorbent and CO_2, while chemisorption takes place by forming bonds either chemical or ionic. Because of the bond forming characteristics, chemisorption is accompanied by high value of Q_{st}. As amine functionalized materials show strong interaction with CO_2 because of the formation of carbamates in a reversible fashion, they require much energy input for the reverse reaction, leading to the increase in regeneration cost. Consequently, adsorbents with high CO_2 capacity and low enthalpy are particularly important and receive special attention.

Likewise enthalpy of adsorption, CO_2 adsorption selectivity over other competitive gases (N_2, CH_4, H_2) and moisture is also equally significant to judge the potential of porous materials in both pre-combustion and post-combustion CO_2 capture [13]. Meanwhile, selectivity in CO_2 over other gases can be differentiated based on the pore size and the surface polarity of the adsorbent. Since, CO_2 possess smaller kinetic diameter (3.3 Å) than N_2 (3.64 Å), therefore ultra-small pores and narrow pore size distribution are considerably important to trap CO_2 during CO_2/N_2 separation. Again, surface engineering of the pores by polar groups could endow better interaction between adsorbent and CO_2, since CO_2 possess higher dipole moment (13.4×10^{-40} C. m^2) and polarizibility (29.1×10^{-25} cm^{-3}) than N_2 (moment: 4.7×10^{-40} C. m^2 and polarizibility: 17.4×10^{-25} cm^{-3}). To determine the selectivity of a binary gas mixture, it requires single-component isotherm data considering several adsorption models such as Henry's law or ideal adsorbed solution theory (IAST) [14]. When Henry's law was employed to determine the adsorption selectivity, it is necessary to fit isotherm data with the virial equation (equation (1)) to calculate the Henry's constant (K_H) using the values of virial coefficients (a_0 and b_0) and equation (3). The ratio of Henry's constant ($S_{mn} = K_{Hm}/K_{Hn}$) for different gas components (m and n) produces selectivity.

$$K_H = \exp(-b_0).\ \exp\left(a_0/T\right) \tag{3}$$

Myers and Prausnitz [14] explained the determination of selectivity by IAST method, while imposing some restrictions on the model. Firstly, the gas components must be ideal; secondly, there would be no interaction between adsorbate-adsorbent and finally surface area of adsorbents must be temperature invariable. While considering those assumptions for applying IAST of the gas mixtures, initially the experimental single-component isotherms should be fitted by single-site or dual-site Langmuir-Freundlich model. The adsorption selectivity of binary gas mixtures is then defined by S, as shown in equation (4), where q is the molar loading of component 1 and 2, p is the partial pressure of those components in the binary mixture.

$$S = \frac{q_1/q_2}{p_1/p_2} \tag{4}$$

Meanwhile, recyclability is another key factor to determine the economic feasibility and practical applicability of the porous adsorbents towards large-scale CO_2 adsorption, which is usually being checked in laboratory by measuring multiple times CO_2 uptake ability of an adsorbent. However, in reality, there are several processes which follow the variation in temperature, pressure, CO_2 concentration, chemical environment to measure the regenerability of the adsorbents. In this regard, pressure swing adsorption (PSA) [15], vacuum swing adsorption (VSA) [16] and moisture swing adsorption (MSA) [17] methods are available. PSA is based on lowering the adsorbate pressure to regenerate the porous adsorbent, where the gas molecules are passed through adsorbent bed at high pressure for better interaction with the sorbent, followed by lowering the pressure to remove the weakly binding molecules from the surfaces at a given pressure. VSA is used for regeneration of adsorbents when the adsorption pressure is lower than atmospheric pressure. However, VSA is expensive and is less applicable for large-scale industrial purposes. Recently, moisture swing adsorption (MSA) shows high popularity for its simple scale-up economics which requires only moisture as cheap source for adsorbent regeneration purposes. Using MSV technique, CO_2 binding with adsorbents takes place under dry condition, but release of CO_2 occurs only in presence of moisture.

Therefore, it can be said that large CO_2 uptake capacity, good selectivity of CO_2 than other competitive gases, high chemical and hydrothermal stability could be perquisites to be an ideal adsorbent. The interaction with CO_2 should be optimum without any need of extra energy penalty for regeneration. Additionally, easy scalability, cheap, and fast kinetics of the sorbents must be the other characteristic [13].

In addition to CO_2 adsorption, CO_2 conversion is also equally important for maintaining the carbon equilibrium in the atmosphere. Being cheap and abundant, CO_2 has broad scope of serving as C1 chemistry to produce fuels to meet our energy demands, and importantly it is also a recyclable raw material [18]. Certainly, a vast number of reviews highlight the potential merits and demerits of each CO_2 adsorbents separately, but to our knowledge, no concrete review is available which summarizes each adsorbent collectively and highlights their efficiency as catalyst for CO_2 conversion reactions. This review may provide the opportunity to the researchers to collaborate with diverse groups working on porous materials in the area of materials science to nanochemistry.

2. Promising adsorbents for post-combustion CO_2 capture

Use of aqueous amines as CO_2 absorbent in the existing power plants is disadvantageous because of regeneration problems and their corrosive nature. It requires costly design and high longevity of the system in order to keep them for safe running. In Fig. 2, we have presented a pictorial representation of aqueous amine-based coal fired plant for CO_2 adsorption and separation from acidic gas mixtures. For convenience and cost-effective adsorption and separation of CO_2, porous solids are much better candidates as they can be easily recycled many times. In this context, zeolites [19], activated carbon [20], porous crystalline frameworks [21], porous polymers [22,23] and mesoporous oxides [24] are appropriate, because they possess suitably decorated narrow micropore/ultra-narrow micropores for interaction with CO_2. Unlike amines, CO_2 is predominately adsorbed onto porous solids as a result of physical interaction. Consequently, it requires less energy for recharging the sorbent to its initial stage for reuse. Zeolites, such as 5A and 13X are less expensive than amines and have received remarkable industrial attention owing to high CO_2 adsorption capacity. However, its application is limited in humid condition for CO_2 separation from flue or biogas because of their higher affinity for H_2O. Hence, there is an urgent need of advanced adsorbents which meet excellent CO_2 adsorption capacity, high CO_2 separation selectivity over N_2, CH_4 and water molecules, as well as durable performances in flue gas conditions.

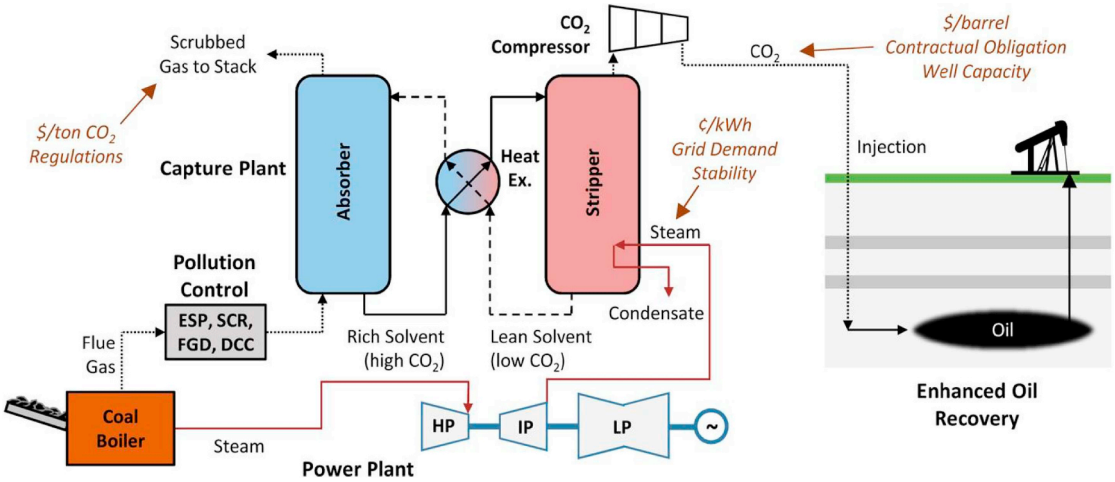

Fig. 2. Schematic representation for flue gas CO_2 capture from coal fired power plant to enhance oil recovery operations, reproduced with permission from Ref. [25].

2.1. Porous coordination polymers

2.1.1. Metal-organic frameworks (MOFs)

Metal–organic frameworks (MOFs) or porous coordination polymers (PCPs) represent a new class of crystallized hybrid porous solid that has promising technological breakthrough with respect to the conventional materials for CCU purposes. It has been reported that MOFs are 3D networks having strong coordination between inorganic and organic units, where inorganic parts are known as Secondary Building Units (SBU) and they can be polyhedra, clusters, chains, layers and the organic linkers are mainly anionic O (polycarboxylates, polyphosphonates) and N (imidazolates, polypyrazolates, polytetrazolates) donors.

Unlike zeolites, MOFs have wide scope for integrating with almost all of the cation in the periodic table. Therefore in the MOFs' structure, a change in combination between metal ions and various organic ligands offer a quasi-infinite possibility of different crystals shapes and chemical compositions that can be easily tuned through controlled variation/coordination of metal centers and length/functionalization of organic moiety. Significantly, the state-of-the art in the design and synthesis of several MOFs is intriguing, offering an ample opportunity in obtaining various MOF structures and properties, which by virtue of synthesis conditions can be post synthetically modified at the requirement for specific applications.

Owing to their tunable pore sizes and high surface area, MOFs are considered as next-generation adsorbent for CO_2. Hence, substantial efforts have been put forwarded by Hagrman et al. [32], Batten et al. [33], Zhou and Kitagawa [34] and Yaghi and co-workers [35] in the last couple of years, specifically to establish MOFs as adsorbents of CO_2, CH_4, H_2 etc. Apart from high CO_2 uptake abilities, MOFs are also useful in selective separation of CO_2 from binary gas mixtures because of their characteristics in controlling the diffusion rate of gases through their narrow channel. Again, the major drawback is the inability to retain the structure during removal of solvent from the pores and thus holds major challenge in designing MOFs for environmental applications [36]. In Fig. 3, we present some representative MOF structures, reported in literature.

2.1.1.1. Impact of surface area on CO_2 uptake. The CO_2 storage capacity of MOFs is being measured at different temperature and pressure, indicating that uptake capacity increases with increasing pressure. Yaghi and co-workers were first to explain the relationship between Brunauer–Emmett–Teller (BET) surface area and CO_2 uptake capacity. Among the several MOFs they studied, MOFs with square channels (MOF-2) [37], MOFs containing open metal sites (MOF-505, $Cu_3(BTC)_2$) [38], interpenetrated MOFs (IRMOF-11) [30], amino and alkyl functionalized MOFs (IRMOFs-3 and 6) [27] are quite promising and potential for CO_2 capture. Significantly, MOF-177 has the high surface area ($4500\ m^2\ g^{-1}$) and possesses high uptake of CO_2 ($13.6\ mmol\ g^{-1}$ at 35 bar) at high pressure [30]. Another ultrahigh porous MOFs were prepared by Furukawa et al. from $Zn_4O(CO_2)_6$ unit, which contain one or two organic linkers. Among them, MOF-210 showed highest BET surface area ($6240\ m^2\ g^{-1}$) and high pore volume ($3.6\ cm^3\ g^{-1}$) reported till date [39]. The ultrahigh porosity of MOF-210 has been achieved mainly because of the expanding organic linkers. As for instance, by extending the size of the 1,3,5-benzenetribenzoate (BTC) in MOF-177, while replacing with larger 4,4′,4”-(benzene-1,3,5-triyl-tris(benzene-4,1-iyl)) tribenzoate (BBC), MOF-200 was obtained with much higher surface area than that of MOF-177 [40]. Strikingly, MOF-200 shows ~16.2 $mmol\ g^{-1}$ CO_2 uptake capacity at 25 °C, 50 bar, which is considered as new record among all solid porous materials. Another Zn-based MOF, UMCM-1, synthesized using larger ligands like H_3BTB and H_2BDC by Koh et al. [41] shows high specific surface area ($4100\ m^2\ g^{-1}$) and large pore volume ($2.141\ cm^3\ g^{-1}$). CO_2 uptake capacity of UMCM-1 has been measured and estimated to be $2.35\ mmol\ g^{-1}$ at 24 bar and 25 °C. In Table 1, we have summarized the important aspects of some MOFs regarding their CO_2 uptake and selectivity in CO_2/N_2, CO_2/CH_4 separation.

For CO_2 capture at ambient condition, *i.e.*; more relevant to flue gas, CO_2 capture is not only influenced by surface area, but also depends on adsorbent-CO_2 interaction. Regarding this, Mg-MOF-74 [Mg_2(DOT)] with an open framework of Mg^{2+} sites demonstrates high CO_2 storage capacity of $8\ mmol\ g^{-1}$ at 25 °C, 1 bar [40]. In this context, it is significant to mention that MOFs with open metal sites are mandatory in achieving high CO_2 storage capacity. Nevertheless, MOFs are significant for CO_2 capture, owing to wide diversity in its structure with high surface area [42] and tailorable material properties towards adsorption of specific gas molecules [43].

2.1.1.2. Effect of water on MOFs during CO_2 uptake. During the activation of MOFs at elevated temperature, solvent molecules coordinatively bound to metal centre were also removed, resulting in coordinatively unsaturated open metal sites in MOFs, which are benefited with good CO_2 uptake property. Since water also coordinates open metal sites in MOFs, therefore there would be a competitive adsorption between water and CO_2. It has been observed that water can easily occupy the open metal sites and accelerates CO_2 adsorption in some MOFs. In this respect, Yazaydin et al. [44] demonstrated that water molecules coordinated to open metal sites of Cu-BTC (HKUST-1), leading to a significantly increases in its CO_2 uptake property than that of dehydrated Cu-BTC framework. A detailed analysis thus revels that the interaction between the quadrupole

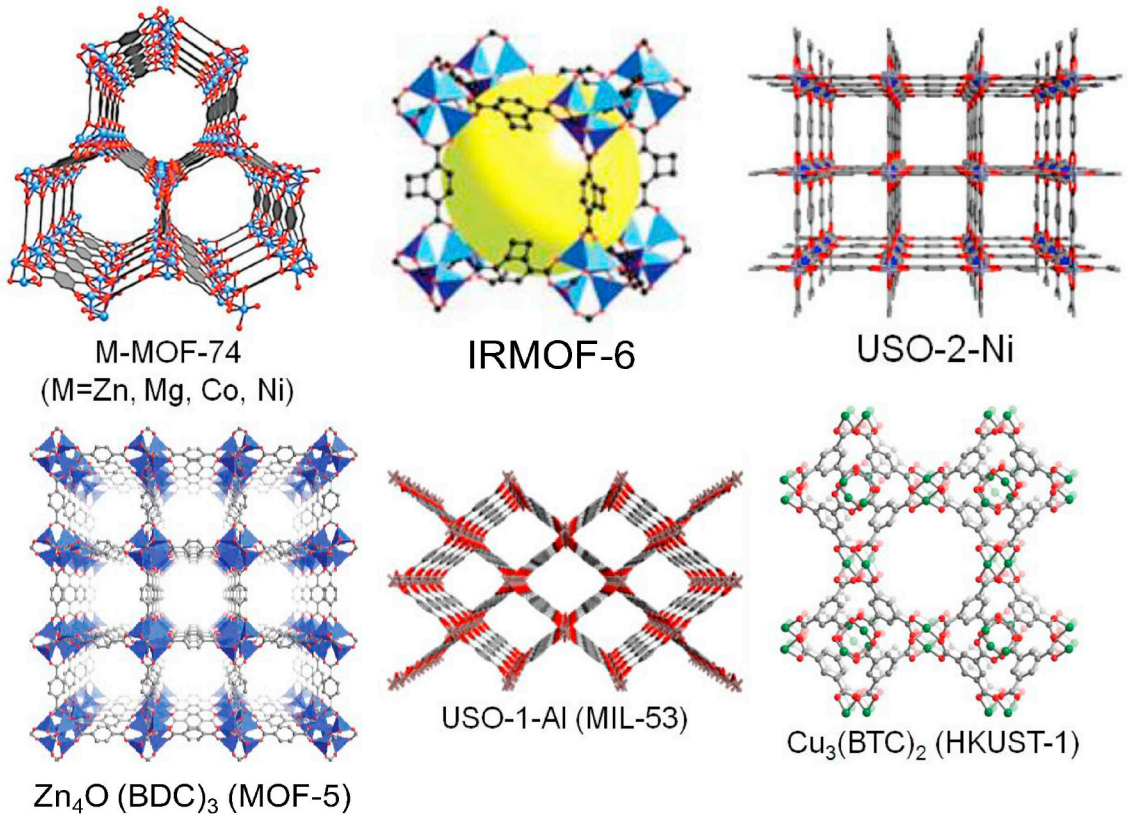

Fig. 3. Crystal structures of several MOFs e.g.; M-MOF-74 [26], IRMOF-6 [27,28], USO-2-Ni [29], MOF-5 [30], MIL-53 [31], HKUST-1 [30] taken with permission from the corresponding references.

moment of CO_2 and the electric field generated by water is solely responsible for the enhanced CO_2 uptake. Furthermore, open metal site contains excess residual charge in MOFs for coordination with polar molecules. The authors clearly explained the phenomenon by calculating the interaction energies between CO_2 and Cu-BTC (both hydrated and dehydrated form), given in Fig. 4a. The result indicates that with the introduction of coordinated water molecules to Cu-BTC, columbic energy increases more than that of non-columbic energy. Therefore, the columbic interaction between water and CO_2 is accountable to the increase in CO_2 adsorption. The interaction between CO_2 and Cu-BTC favors only when water molecules occupy the Cu open-metal site.

In other cases, water could only destroy the MOF structure and shows a detrimental effect on CO_2 adsorption. Kizzie et al. [46] showed the humidity effect on the CO_2 capture performance of M/DOBDC series of MOFs (M = Zn, Ni, Co and Mg), where significant decrease in the CO_2 uptake capacity was observed for Mg/DOBC and Zn/DOBC. In another report, Liu et al. [47] also highlighted the effect of water on the stability and application of various MOFs.

Again, breathing effect is an interesting phenomenon in MOF crystal, which is induced by the adsorption of water molecules, as observed in MIL-53 (Al) and MIL-53 (Cr) (Fig. 4b). In the hydrated form of MIL-53 (left), the pores are deformed because of hydrogen bonding interactions between the oxygen atoms of carboxylates/hydroxyl groups of MOFs and hydrogen atom of water. After removal of water through heating, the pore returns back to the structure with more open porosity, shown in the right side image of Fig. 4b. Bourrelly et al. [45] found that the shrinkage in structure could be due to the adsorption of CO_2 to the hydroxyl groups in MIL-53, which reopens with increasing CO_2 pressure. It is noticeable that MIL-53 (Al) and MIL-53 (Cr) have CO_2 adsorption capacity of 10.4 mmol g^{-1}, which is higher than conventional zeolites and is also comparable with microporous carbon. Later, Thallapally et al. [48] synthesized interpenetrated MOFs having breathing motion upon solvent loss and CO_2 inclusion. This breathing MOF shows 7.1 mmol g^{-1} CO_2 uptake capacity at 30 bar and 25 °C, similar to NaX zeolites under same conditions. A steam stability map is shown in Fig. 5, suggesting that the stability of MOFs increases with increasing coordination number of metal atoms from 4 to 6.

On the other hand, MOFs as HKUST-1 [49] is stable in O_2 at 25 °C, but its crystallinity gets reduced in humid condition, suggesting that moisture could hamper the coordination environment of open metal sites present in MOF. As a result, CO_2 adsorption capacity of HKUST-1 was progressively reduced upon its cyclic exposure to 30% relative humidity. It was also reported that HKUST-1 and Ni/DOBDC are prone to lose carbon dioxide capacity after repeated H_2O/CO_2 mixed treatment. Although, MOF-177 is quite well known for high pressure CO_2 storage, it collapses upon water adsorption and decomposes while expose to ambient air within 3 days. Recently, Kizzie et al. [50] also reported that the CO_2 uptake capacity of Mg/DOBDC can be diminished after water breakthrough and subsequent regeneration. Hence, it can be said that water vapor has huge impact on MOF structures by influencing towards CO_2 adsorption.

2.1.1.3. Strategies that enhance CO_2 capture. In order to consider MOFs as an ideal adsorbent, several important features need to be considered since they could increase uptake capacity as well as selectivity. As for instance, pore size modification would be crucial, because a slight variation in pore size can change uptake amount as well as heat of affinity of CO_2. Not only pore sizes, chemical bonding interaction between CO_2 and MOF crystal structure might be pivotal in tailoring CO_2 uptake capacity. Herein we describe several important features that are crucial in this regard.

Table 1
CO_2 uptake properties including CO_2/N_2 and CO_2/CH_4 selectivity of various adsorbents.

Name	BET Surface Area ($m^2 g^{-1}$)	CO_2/mmol g^{-1}			P (bar)	Q_{st} (kJ mol^{-1})	CO_2 Selectivity		Ref
		0 °C	25 °C	> 25 °C			CO_2/N_2	CO_2/CH_4	
MOFs									
$Cu_2(abtc)_3$ (SNU-5)	2850	8.75			1				[163]
$Cu_2(bdcppi)(DMF)_2$ SNU-50	2300		3.1		1				[164]
$Dy(BTC)(H_2O)$. DMF	655	6.2			1				[165]
$Al_4(OH)_2(OCH_3)_4(BDC\text{-}NH_2)_3$	1268	5.5			1				[166]
Amine-MIL-101 (Cr)	2297		2		2				[167]
					1			10 (50 °C)	
Amine-MIL-101 (Cr)-50% PEI-amine	946.8		4		2				
					1			100 (50 °C)	
Amine-MIL-101 (Cr)-75% PEI-amine	243.3		3.5		2				
					1			1030 (50 °C)	
$Zn_2(BTetB)$	1370	4.5			1				[168]
$[In_3O(diazDBC)_{1.5}(H_2O)_3](NO_3)$	892	4.0			1	28.5			[169]
Cu-BTTri-mmen	870		15.4		1	96			[170]
$Co_4(OH)_2(p\text{-}CDC)_3$	1080	3.7			1				[171]
$Cu(bpy)_2(BF_4)_2$	390	3.1			1	12.2			[172]
$Cu_2(bptb)$	1217*	2.8			1				[173]
Zn-carborane	800	3.1			1				[174]
$Ni_2(bpy)_3(NO_3)_4$		2.4			1				[175]
$Cd(mim)_2$	2420	1.3			1				[176]
HKUST-1 (CuBTC)	1270			17.5 (35 °C)	300	29.2			[177]
HKUST-1						35[d]			[178]
						30			[179]
					1			6 (35 °C)	[180]
MOF-200	6240		54.5		50				[39]
MOF-505	1547		10.2		35				[30]
IRMOF-1 (MOF-5)	3000				2			29[c] (35 °C)	[181]
						34			[182]
IRMOF-16-4Li					10			75 (25 °C)	[183]
TBA@bio-MOF-1	830			1.3 (40 °C)	1				[64]
TEA@bio-MOF-1	1220			1.54 (40 °C)	1				[64]
TMA@bio-MOF-1	1460			1.52 (40 °C)	1				
bio-MOF-1	1680			1.2 (40 °C)	1				
MIL-53(Cr)				1.93 (31 °C)	1				[31]
IRMOF-3	2160			1.1 (40 °C)	1				[28]
soc-MOF						28.5			[169]
$Zn_2(BDC)_2(4,4'\text{-bpy})$						19			[184]
Cu-BTTri-en						90			[7]
MIL-100 (Cr)						62			[185]
TBA@bio-MOF-1						55			[186]
bio-MOF-1						35			
bio-MOF-11						45			[64]
ZIFs									
ZIF-8	880		0.7		1		1.91[b]		[82]
						15.9[d]			[187]
ZIF-8, Matrimid polymer					2.7		23-30 (35 °C)		[188]
ZIF-68					1		18.7 (25 °C)	5 (25 °C)	[70]
ZIF-78					1		50.1 (25 °C)	10.6 (25 °C)	
ZIF-81					1		23.8 (25 °C)	5.7 (25 °C)	
ZIF-82					1		35.3 (25 °C)	9.6	
ZIF-95					1		18 (25 °C)	4.3 (25 °C)	
ZIF-69						22.7[d]			[187]
ZIF-76						25.1[d]			
POPs									
TAPOP-1	930	3.5			1				[189]
TAPOP-2	940	3.1			1				
NOP-51A	1071	3.0			1				[190]
PECONF-1	499	1.86	1.34		1	29	135[a]		[191]
							51[b]		
PECONF-2	637	2.8	1.98		1	31	44[b]		
PECONF-3	851	3.5	2.47		1	26	41[b]		
PON-1	1422		2.61		1				[104]
PON-2	168		0.77		1				
PON-3	51		0.86		1				
PAF-33	821	2.16	1.25		1	27.4	19.4[b]		[192]
PAF-33 (-NH_2)	370	1.19	0.75		1	32.9	79.8[b]		
							104.3[b]		
PAF-33 (-COOH)	445	1.94	1.21		1	30.0			

(*continued on next page*)

Table 1 (*continued*)

Name	BET Surface Area ($m^2 g^{-1}$)	CO_2/mmol g^{-1}			P (bar)	Q_{st} (kJ mol^{-1})	CO_2 Selectivity		Ref
		0 °C	25 °C	> 25 °C			CO_2/N_2	CO_2/CH_4	
PFPOP-1	570	3.34	1.4		1	27	43.7[a]		[103]
PFPOP-2	630	4.11	1.86		1	30	52[a]		
PFPOP-3	530	4.74	2.0		1	32.5	56.5[a]		
CMP-1 (-COOH)	522	1.60			1				[23]
CMP-1 $(-CH_3)_2$	900	1.62			1				
CMP-1 $(-OH)_2$	1043	1.80			1				
TCMP-0	963	2.4	1.3		1		9.6[b]		[112]
TCMP-2	995	2.6	1.4		1		7.6[b]		
TCMP-3	691	2.25	1.3		1		25[b]		
TCMP-5	494	1.22	0.7		1		17.0[b]		
Fe-POP-1	875	5.21							[116]
Fe-POP-2	855	5.10							
Fe-POP-3	750	2.50							
PPN-6	4023		1.4		1	17			[193]
PPN-6 (SO_3H)	1254		3.6		1	30.4	155[a]		
PPN-6 (SO_3Li)	1186		3.7		1	35.7	414[a]		
PPN-6 (SO_3NH_4)	593	7.5	3.7		1	40	196[b]		[194]
PPN-CH_2-DETA	555			2.3 (40 °C)	0.15				[193]
PAF-26 (COOH)	717	2.3	1.4		1	28	20[a]		[195]
PAF-26 (COOLi)	592	2.5	1.6		1	32	24[a]		
PAF-26 (COONa)	483	2.7	1.6		1	35	53[a]		
PAF-26 (COOK)	430	2.4	1.5		1	33	50[a]		
PAF-26 (COOMg)	572	2.8	1.7		1	30	73[a]		
TRITER-1	716	13.4			5	38.1			[196]
			3.12		5				
HPF-1	576			2.8 (30 °C)	1		120[a]		[107]
COP-33	53.20		1.44	0.98 (50 °C)	10		4:1[c] (50 °C)	4:1[c] (50 °C)	[83]
COP-32	46.00		1.11	0.80 (50 °C)			20:1[c] (50 °C)	20:2[c] (50 °C)	
COFs									
COF-103	3530	1.39			1				[128]
			27		55				
COF-102	3620	1.38			1				
			27.3		55				
COF-10	1760	1.02			1				
			23.0		55				
COF-8	1350	1.2			1				
			14.3		55				
COF-6	750	1.4			1				
			7.05		55				
COF-5	1670	31			1				
			19.7		55				
TDCOF-5	2050	2.09			1	21.8			[132]
TpBD (NO_2)	295	2.3			1				[197]
TpBD $(-CH_3)$	468	1.65			1				
TpBD $(-OCH_3)$	330	1.2			1				
NTU-COF-2	1619	2.3			1	27			[144]
CTF-1	746	2.45			1	27.5	20[a]		[198]
CTF-1-600	1553	3.6			1	30	13[a]		
FCTF-1	662	4.7			1	35	31[a]		
FCTF-1-600	1535	5.53			1	32	19[a]		
COF-JLU2	415	5			1	31	77[b]		[199]
ACOF-1	1176	4.02			1	27.6	40[b]		[200]
ILCOF-1	2723	1.4			1	18.3			[141]
			29.3		40				
APTES-COF-1	490			1.02 (30 °C)	1				[141]
				4.02 (30 °C)	37				
Porous oxides									
Mesoporous alumina with polyethylenimine				2.7 (75 °C)	1				[201]
Activated alumina (commercial)				1.82 (100 °C)	1				[202]
SBA-15-TA	182	1.6		1.45 (40 °C)	0.99				[203]
SBA-15-DA	235	1.77		1.39 (40 °C)	0.99				
SBA-15-AP	380	1.52		0.99 (40 °C)	0.99				
MgO	28			1.8 (50 °C)	0.15				[204]
				0.9 (100 °C)	0.15				
SM-20	567	2.11	1.65		1	32.5			[205]
SM-10	968	2.61	1.80		1	20.0			
Mesoporous MgO				2.27 (100 °C)	1				[206]
CaCoAlO				1.39 (350 °C)	1 (8% CO_2)				[207]
MgAlO				1.13 (350 °C)	1 (8% CO_2)				
MgAl-HT-550				1.18 (400 °C)	1 (15% CO_2)				[208]

(*continued on next page*)

Table 1 (*continued*)

Name	BET Surface Area ($m^2 g^{-1}$)	CO_2/mmol g^{-1}			P (bar)	Q_{st} (kJ mol^{-1})	CO_2 Selectivity		Ref
		0 °C	25 °C	> 25 °C			CO_2/N_2	CO_2/CH_4	
SBA-15	717		3		10				[209]
APTES@SBA-15	344		2.3		10				
$AlPO_4$-25		1.25			1		45.6[b] (0 °C)		[210]
$AlPO_4$-53		2.25			1		76.4[b] (0 °C)		
Zeolite									
Zeolite 13X	710			0.7 (120 °C)	1				[211]
WE-G 592	625			0.6 (120 °C)	1				
APG-II	710			0.38 (120 °C)					
Zeolite 5A		4			10				[212]
				2.5 (70 °C)	2				
		3.5			1				
Zeolite 13X	585.5			3 (50 °C)	1				[213]
Zeolite 13X with added Monoethanolamine				0.8 (75 °C)	0.15				[214]
Zeolite 13X with added Isopropanolamine				0.5 (75 °C)	0.15				
Zeolite ITQ-2 with added 3-Aminopropyl trimethoxysilane)		2.13			1				
β-Zeollite				1.4 (30 °C)	1				
Zeolite-chitosan composite	22.53		1.7		4.6				[215]
Zeolite NaX	183		2.72			31–37	146[a] (23 °C)		[216]
Cs@RWY	526		3.21			30.2–32.1	180[a] (0 °C)		
Zeolite 13X	726		4.7		1	40	30.4		

[a] IAST selectivity.
[b] Henry's law selectivity.
[c] Selectivity was calculated from single gas sorption data.
[d] Simulated heat of adsorption; *Langmuir surface area.

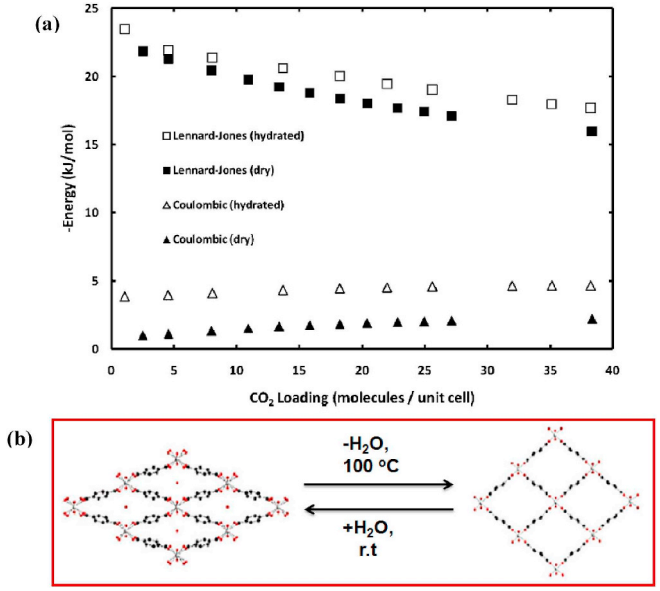

Fig. 4. (a) Simulated interaction energies between CO_2 and Cu-BTC crystal (both dry and hydrated) at 298 K, taken with permission from Ref. [44]; (b) Hydration and dehydration process occurring in MIL-53 (Al, Cr). Left: hydrated structure; right: dehydrated structure. Reproduced with permission from Ref. [45].

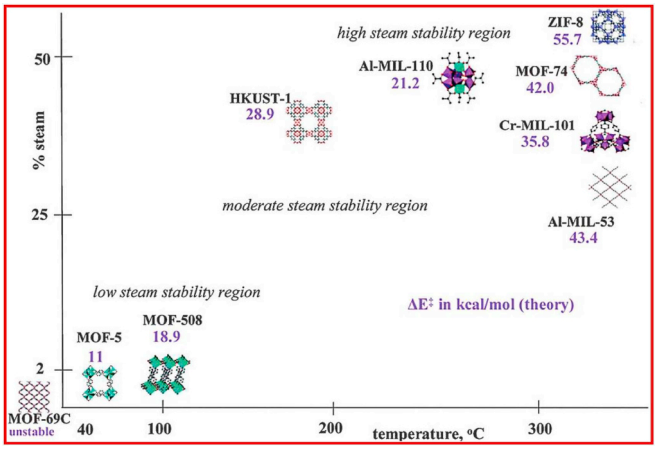

Fig. 5. Steam stability map for several MOFs. The position of the structure for a given MOF suggests its maximum structural stability, determined by XRD. The figure is taken with permission from Ref. [51].

2.1.1.3.1. Interpenetration in MOF frameworks. Since interpenetration of two frameworks reduces pore volume, therefore, it considers as an obstacle for the formation of highly porous frameworks. Thus, interpenetration has been treated to reduce the pore dimensions (Fig. 6) of IRMOFs e.g. IRMOF-9, IRMOF-11, and IRMOF-13, which show larger CO_2 selectivity over other gases than their non-interpenetrated MOF counterparts, as observed by Keskin and Sholl [52]. Again, Cheon et al. [53] also prepared a doubly interpenetrated Mg-based porous MOF with 3D channels, *i.e.* SNU-25, which exhibits high thermal stability and high selectively of CO_2 over CH_4. The effect of interpenetration is largely observed in CuTATB-60 as interpenetrated MOF having higher surface area and higher stability than their non-interpenetrated counterpart, CuTATB-30 [54]. Again, CuTATB-60 exhibits superior CO_2 uptake ability (4.3 mmol g^{-1}) with privileged CO_2/N_2 separation selectivity (20:1) than that of CuTATB-30. Therefore, all these study justifies the requirement of interpenetration in MOF crystal to tailor high selective adsorption of CO_2.

2.1.1.3.2. Electrostatic and hydrogen bonding interaction between CO_2 and MOF crystal. It can be said that electrostatic interaction between MOFs and CO_2 could originate high CO_2 uptake property. Electrostatic forces in MOFs can be enhanced through doping and by modifying with polar species. Babarao et al. [56] demonstrated that the presence of extra framework ions could be suitable to enhance the interactions with guest molecules and can act as an additional adsorption site. Not only this, polar ion is suitable to increase higher CO_2 selectivity over other gases, as observed in charged soc-MOF than IRMOF. Botas et al. [57] demonstrated that Co doped IRMOF-1 has higher CO_2 adsorption

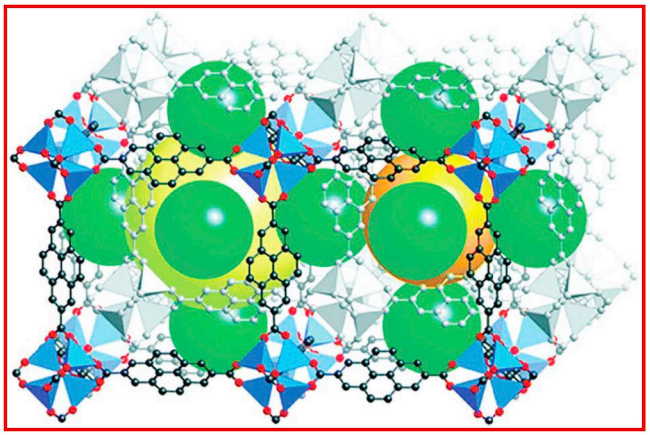

Fig. 6. Diagrammatic representation of the pore structure in IRMOF-13; the catenation of two frameworks, one shown in grayscale, reduces the fixed diameters of the large and small pores defined by either framework alone. Additional smaller voids are formed, shown as green spheres, which account for roughly 45% of the pore volume. Atom colors: C: black; O: red; Zn: blue tetrahedra; H not shown, taken with permission from Ref. [55]. (For interpretation of the references to color in this figure legend, the reader is referred to the Web version of this article.)

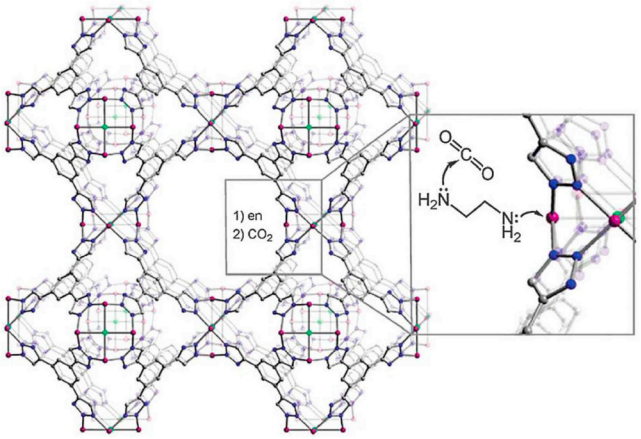

Fig. 7. A Cu-based MOF shows surface functionalization of coordinatively unsaturated Cu-sites with ethylenediamine. The amine site shows additional attack with CO_2 during CO_2 uptake experiment. Purple, green, gray, and blue spheres represent Cu, Cl, C, and N atoms, respectively; framework H atoms are not seen. Reproduced with permission from Ref. [62]. (For interpretation of the references to color in this figure legend, the reader is referred to the Web version of this article.)

capacity at high pressure than that of Co-free sites. Their study shows the possibility of doping MOFs with various metal ions during solvothermal crystallization. Accordingly, carbon nanotube modified with HKUST-1 exhibits improved CO_2 uptake capacity upon optimum loading with Li as secondary metal, because too high concentration of Li ultimately causes the destruction of the framework structure. Again, solvent exchange with polar groups can also be utilized for favoring CO_2 adsorption, as observed in Zn-paddlewheel MOF, where the coordinated solvent molecules are replaced by polar 4-(trifluoromethyl) pyridine as ligand and this modification introduces electrostatic forces into MOF structure for considerable improvement in selective uptake of CO_2 [58].

Apart from electrostatic interaction, hydrogen bonding between MOFs and CO_2 can also be encouraging for executing high CO_2 uptake phenomenon. In this regard, Ramsahye et al. [59] suggested that owing to the presence of μ_2-OH in MIL-53 (Al) and MIL-53 (Cr), they could exhibit hydrogen bonding with CO_2, which favors > 40 kJ mol^{-1} heat of adsorption. Vimont et al. [60] gave spectroscopic evidences for the formation of donor-acceptor complex between CO_2 molecule and hydroxyl groups. In contrast to electron withdrawing MOFs, electron donating MOFs could interact better with CO_2 by forming donor-acceptor complexes.

It is noteworthy that MOFs with organically modified by amines, shows substantial chemical bonding interaction with CO_2, that have been studied by many researchers. Vaidhyanathan et al. [61] prepared amine functionalized MOF using zinc carbonate, 3-amino-1,2,4-triazole and oxalic acid. The 3D network that forms while pillaring of Zn-aminotriazolate layers by the oxalate groups, can sufficiently expose free amine sites for further interaction with CO_2 at low pressure with 40.8 kJ mol^{-1} heat of adsorption. Additionally, Demessence et al. [62] explored the effect of amine functionality in MOF frameworks for low pressure (< 1 bar) CO_2 adsorption. They showed that ethylenediamine functionalized MOF had greater CO_2 adsorption capacity of 0.366 mmol g^{-1} than the non-functionalized MOF (0.277 mmol g^{-1} at low pressure, 0.06 bar) and displayed superior isosteric heat of adsorption (90 kJ mol^{-1}) than non-amine functionalized MOF (21 kJ mol^{-1}). A Cu-based MOF with pendant alkylamine functional site is presented in Fig. 7.

In addition to direct synthesis of amine-MOFs, post-synthetic modification of MOFs with amino site is also useful for CO_2 storage. In this way, Zn(II)-based paddle-wheel MOFs having anhydride sites can be readily converted to the corresponding amides, as reported by Cohen and co-workers [63]. Other amine MOFs, *e.g.*; Adenine-based MOF, bio-MOF-11 were reported by Rosi and co-workers [64], show high CO_2 selectivity over N_2 on account of favorable interaction between CO_2 and Lewis basic amino and pyrimidine groups of adenine, together with narrow distribution of small pores. Furthermore, bio-MOF-11 has been post synthetically modified with TMA, TEA, and TBA cations in the pore wall for improving CO_2 adsorption. Therefore, we foresee this amine functionalized MOFs can be better utilized for capturing CO_2 significant to real world applications. However, for practical applications, the utilization of MOFs for CO_2 capture in moist condition is questionable. Hence, zeolitic imidazolate frameworks (ZIFs) [65,66] could be befitted as better adsorbents than MOFs because of their higher CO_2 selectivity over water, allowing the adsorbents to store more carbon before reaching saturation [67].

Despite many advantages of the above-mentioned MOFs in carbon capture purposes, cost of MOF is still a major drawback that impedes its large-scale applications in industry. Similar to zeolites, MOFs are also synthesized by hydrothermal or solvothermal ways, which includes energy requirement and the cost of reactors. Again, the use of extended and rigid organic linkers, metal salts, non-reusable organic solvents adds much cost in the synthesis process. Additionally, the separation and the activation of MOF through solvent exchange process are energy intensive. It can be said that MOFs synthesis does not require a total capital investment, but rely on simply precipitation and crystallization methods. However, the main challenge is to utilize aromatic carboxylic, hydroxyl and amine ligands as most of these ligands are not commercially available in large-scale and require extra effort for their preparation. Therefore, MOFs prepared from cheap and abundant ligands would be highly desirable for their commercial applications. Another alternative to solvent exchange process is “super critical” drying, which activates MOFs and increases its surface area. This technique is much cheaper than solvent exchange process and can reduce the total cost of the preparation of MOF materials.

2.1.2. Zeolitic imidazolate frameworks (ZIF)

ZIFs are an emerging subclass of MOFs containing imidazole as building unit and consist of M-Im-M linkages (M stands for Zn, Co cations and Im for the imidazole linker). In 2003, D. Y. Zhao group [68] introduced ZIF as analogous to MOF materials because of their identical topology. ZIFs have structural similarity with conventional aluminosilica zeolites, where Zn^{2+} is analogous with Si and the ligand imidazole

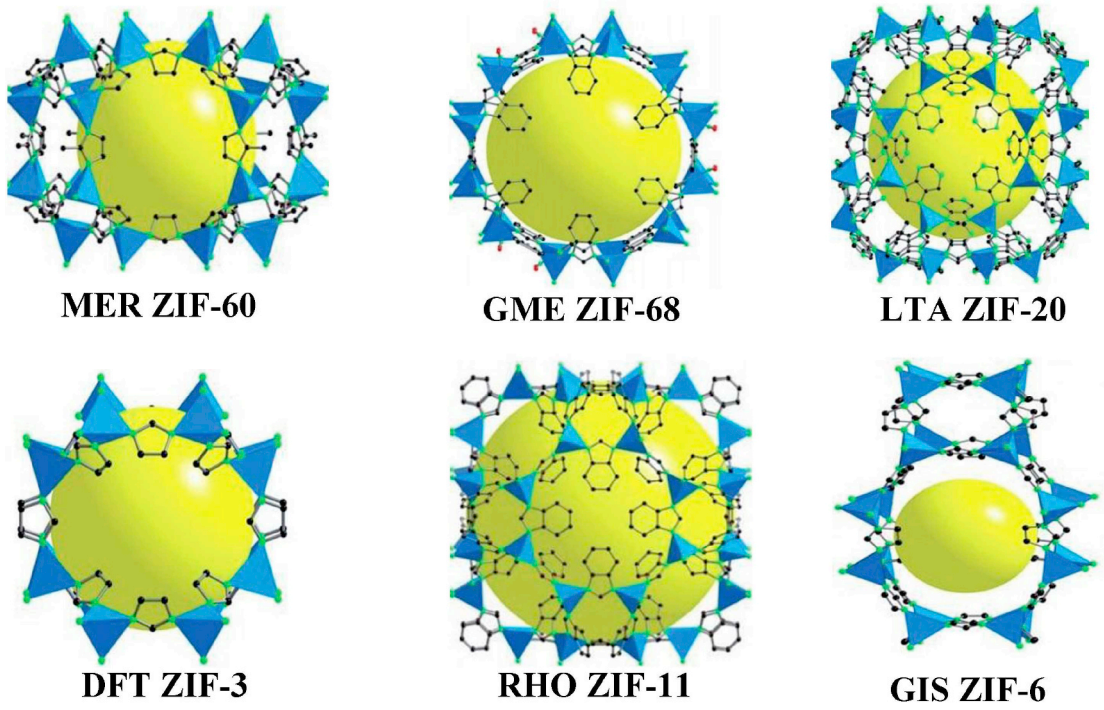

Fig. 8. Crystal structures of some significant ZIF frameworks (the first three capital letters under each example stand for the zeolite structure code), taken with permission from Ref. [70].

that is bridged with metal ions mimic the role of oxygen in zeolites. In ZIFs, M-Im-M bond angle is 145° that is resemblance with O-Si-O bond angle of zeolites and thus they are topologically similar with zeolites also [69]. ZIFs possess the combined characteristic advantages of both MOF and zeolite, such as ultrahigh surface area, narrow distribution of pores, enriched with organic functional sites, easy to modification and high thermal and chemical stability. Henceforth, ZIFs are unique to MOFs and hold great potential in gas adsorption and separation. In this field, O. M. Yaghi and others contributed significantly for the development of interesting ZIF frameworks and their potential applications as CO_2 storage [70,71]. In this review, we have demonstrated some ZIF-based adsorbents as alternative to MOFs for selective adsorption of CO_2. Fig. 8 shows some representative ZIF structures.

2.1.2.1. Structure property relation for CO_2 adsorption. Adsorption sites within ZIFs are associated with the ligand and the metal centre. Contrary to MOFs, gas adsorption in ZIFs is less dependent on metal-adsorbate interaction because of insufficient free space near zinc metal centre, as demonstrated by DFT calculation for H_2 adsorption in ZIF-8 [72]. This is supported by the fact that ZnO_4 tetrahedra in MOF-5 do not exhibit the restricted configuration and hence adsorption occurs near the metal sites. Because of the high steric congestion around the metal sites in ZIF, gas adsorption near the ZIF metal clusters is hindered. The most effective way to modify CO_2 adsorption capacity and selectivity is by regulating the materials topology and organic substituent. Since the discovery of ZIFs, a large number of ZIF materials show CO_2 adsorption capacity up to 3.12 mmol g^{-1} at 0 °C [70]. In general, topologies with greater specific surface area result in higher adsorption because of more van der walls sites to interact with CO_2. As for example, rho-ZIF and sod-ZIF [73] synthesized from same ligand (4,5-imidazoledicarboxylic acid) have different BET surface area and pore volume but hold almost equivalent CO_2 adsorption capacity at 1 bar and 0 °C. However, at higher pressure, rho-ZIF exhibits 25% greater loading of CO_2 than sod-ZIF because of larger pore volume of rho-ZIF. Morris et al. [74] experimentally showed that pore size of sod-ZIF is closer to the critical size of CO_2 for having greater interaction potential, which is helpful for CO_2 adsorption at low pressure, but at higher CO_2 pressure, available pore volume is a limiting factor and the more open topologies of rho-ZIF could exhibit higher loading. Thus, one needs to consider topology is a key-factor while designing ZIF structures.

2.1.2.2. Effect of water. Water vapor plays a detrimental role during CO_2 adsorption of an adsorbent; therefore it should be judged prior to any practical usage of the material. Zeolites have significantly high affinity towards moisture, which limits their use in CO_2 separation from flue-gas condition. Despite having topologically similar with zeolites, ZIFs are practically hydrophobic and are extremely stable in boiling water condition for several days in contrast to certain MOFs that are even decomposed in moisture present in air [75]. High water stability of ZIFs is probably due to the metal-ligand coordination in the framework, which may be coordinatively substituted by water and retains the stability. ZIF-90 with hydrophilic ligand can store > 20 mmol g^{-1} water vapor at 308 K, while hydrophobic ZIFs (ZIF-8 and ZIF-71) show no water adsorption phenomenon. Theoretically, it has also been demonstrated that the effect of topology and the presence of hydrophobic ligands can control the overall water uptake in ZIFs [76]. It can be said that ZIFs are viable candidates for post-combustion CO_2 capture without being affected in presence of water and demonstrate their high selectivity in the desired gas separation purposes.

2.1.2.3. ZIFs as CO_2 adsorbent. ZIFs are more appropriate for practical applications because of their better thermal and chemical stability than MOFs as well as their synthesis opportunity in water. For cost-effective designing of materials, it would be striking if organic solvent can be replaced by water. In this regard, S. Aguado and co-workers [77] have developed an easily scalable with high yield (79% based on Zn) synthesis of ZIF-93 in aqueous condition and at room temperature, where ammonia is used as an additive. This reported ZIF shows CO_2 adsorption capacity of ~8.0 and 1.6 mmol g^{-1} at 30 and 1 bar respectively, which is comparable with ZIF-93 prepared in DMF solvent. This finding clearly has a merit as it encourages the use of water as eco-friendly solvent at room temperature.

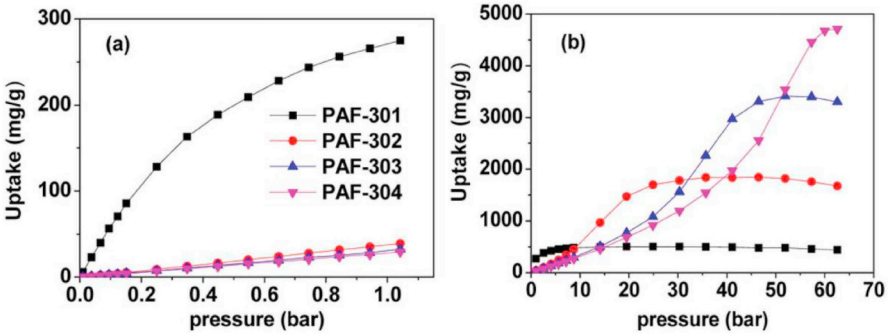

Fig. 9. CO_2 adsorption isotherms at 298 K in PAFs: (a) at low pressure; (b) at high pressure, reproduced with permission from Ref. [91].

Accordingly, ZIF-8-based membrane is also prepared for selective CO_2 adsorption. Song et al. [78] reported the syntheses of ZIF-8 membrane by dispersing ZIF-8 nanoparticles into the polymer of Matrimid 5218 polymer, which increases the permeability of CO_2 during the pure gas sorption because ZIF-8 provides much larger free volume than neat polymer [79]. Besides the above mentioned properties, ZIF-8 is thermally more stable than commercially available Zeolite-13X. To increase CO_2 adsorption efficiency, post-synthesis modification of ZIF-8 with ethylenediamine is considered for better interaction with CO_2 and improved uptake efficacy than ZIF-8 itself at 25 °C and 25 bar [80]. Simulated CO_2 adsorption capacity of several amine modified ZIF-8 has been reported by Liu et al. [81]. They illustrated that CO_2 adsorption is proportional to the amine loading in the adsorbent and explained by both experimental and theoretical studies, which can enrich researchers for better designing of ZIF-8-based membranes for CO_2 adsorption in future.

In another report, Gao et al. [82] introduced high hydrophobic zeolite@ZIF-8 composites to investigate CO_2 capture efficiency in presence of water. They prepared hydrophobic zeolite@ZIF-8 by combining a pre-seeding process and a two-step temperature controlling crystallization processes, while introducing ZIF-8 into commercial zeolite adsorbent (5A) core. 5A@ZIF-8 composite exhibits a dynamic hydrophobic hindrance effect for the separation of CO_2 from the simulated humid flue gas (15% CO_2 and 90% humidity at 298 K) and it has 2.67 mmol g^{-1} CO_2 uptake capacity with CO_2/H_2O selectivity of 6.61. This process significantly improved the surface hydrophobic properties by simply introducing a porous hydrophobic shell on an inexpensive commercially available adsorbent to form a core-shell structure. Nevertheless, the preparation cost of ZIFs is mainly dependent on the imidazole derivatives which can only be synthesized in research labs in laboratory scale. Therefore, implementation of the expensive ZIFs for commercial applications in large scale is lagging far behind.

2.2. Porous organic polymers (POPs)

2.2.1. Covalent organic polymers

POPs exists as both amorphous and crystalline forms, where the frameworks are constructed by lighter elements (C, H, O, N) and are associated with strong covalent bonds [83–85]. A series of exciting characteristics observed in POPs *viz.* high-specific surface area, good physicochemical stability, tunable pore dimensions, topologies, and chemical functionalities, make them promising adsorbents for CO_2 capture.

Different POPs are reported in the literature, *e.g.;* porous polymer networks (PPNs), polymers of intrinsic microporosity (PIMs), conjugated microporous polymers (CMPs), hypercrosslinked polymers (HCPs), crystalline triazine-based frameworks (CTFs), porous organic frameworks (POFs) and porous aromatic frameworks (PAFs) [86–88], where the state-of-the art development in the design, synthesis, characterization and the CO_2 adsorption performances has been discussed. It is worthy to mention that POP surfaces can easily be controlled in favor of CO_2 adsorption through tailoring its surface property (surface area and pore size) and incorporation of basic substitutions. Thus understanding of all these aspects could lead to the development of new possibilities of novel frameworks that target high CO_2 adsorption. In this context, fabrication of POPs from rigid/robust monomers through several advanced C-C bond forming reactions (Yamamoto, Suzuki, Sonogashira-Hagihara, Ullmann, and Buchwald-Hartwig couplings, click chemistry and various condensation reactions [89,90]) could be perquisites in determining CO_2 adsorption performances. Herein, we describe the critical factors which directly influence the CO_2 uptake efficiency of POPs.

2.2.1.1. Surface area and porous properties of POPs for CO_2 uptake. For CO_2 storage, BET surface area is an important factor, but it is not too significant at low pressure, rather is imperative at high CO_2 pressure as it increases the number of adsorption sites. At very high pressure, all the adsorption sites on the surfaces of POPs are available for CO_2 binding and after monolayer coverage, only additional CO_2 molecule could condense inside the pores, resulting in overall increase in CO_2 sorption capacity. Thus, the excess CO_2 adsorption is directly related to pore volume as well as BET surface area, suggesting that the synthesis of high surface area POPs are desirable for high pressure CO_2 uptake.

For a series of PAF frameworks, Cao and co-workers [91] have theoretically studied how CO_2 uptake is related to the linker length. In this study, they showed that with increasing linker length in PAF materials (PAF-30Xs where X = 1, 2, 3, 4 represents the linker length *i.e.*; the number of phenyl rings in the monomer), CO_2 adsorption decreased in the order of PAF-301 > PAF-302 > PAF-303 > PAF-304 at low pressure (Fig. 9a), but at high pressure it follows the reverse order (Fig. 8b), indicating that CO_2 adsorption capacity entirely depends on high and low pressure. Although surface area in PAFs increased as PAF-304 > PAF-303 > PAF-302 > PAF-301, but PAF-301 shows highest CO_2 uptake capacity at low pressure, clearly suggesting that small pores lead to strong interaction with CO_2 and increase heat of adsorption, which all are dominating at low CO_2 pressure. At very high pressure (> 50 bar), CO_2 adsorption reaches to saturated value and shows entirely opposite relationship of PAF series, indicating that surface area and pore volume dominate the saturated CO_2 adsorption/sequestration capacity. Herein, we describe some high surface area POPs as CO_2 adsorbents at both high and low pressure (Table 1).

In addition to surface area and functionality of the surfaces, pore size is also a key factor in controlling CO_2 adsorption and selectivity, thus it is essential to tailor the pore size near about the kinetic diameter of CO_2 (3.3 Å) in order to attain maximum efficiency [92]. Based on the difference in polarizabilities between CO_2 and other gases, tuning the pore size of the adsorbent can lead to the enhancement of carbon capture property.

2.2.1.2. Scalability and textural properties. Considering massive CO_2 emission in the atmosphere, large-scale production of functional organic porous materials from inexpensive starting materials and reagents through the bottom-up synthesis approach should be the present need to protect our environment. Furthermore, simple reaction procedures could be ideal for mass production of functional organic porous materials. However, POPs reported so far requires expensive metal catalysts in stoichiometric amounts, demanding operation procedures and additional cost of post-washing steps for removal of unreacted monomers, by-products and high-boiling solvents. Thus, it is mandatory to develop facile polymerization processes to address these critical issues in order to ensure the low cost and scalability of the resulting polymers. Additionally to meet the atom efficiency, liquid phase reaction with minimum number of reagents and catalysts are preferred so that it can be directly used as the precursor for solution processing.

The problems has been well addressed by S. Dai, A. Coskun, L. Fang and colleagues, who prepared the targeted polymers by using acid or elemental sulfur as simple catalysts. S. Dai and others reported the formation of solution-route preparation of polymer film with triazine sites from superacid catalyzed trimerization of aromatic nitriles, which shows 738 $m^2 g^{-1}$ BET surface area [93]. With triazine sites, the polymer film exhibits an increased selectivity for membrane separation of CO_2 over N_2, having CO_2/N_2 selectivity of 29 ± 2 achieved with a CO_2 permeability of 518 ± 25 barrer. Similarly, aldol triple condensation reaction has been used for the mass production of highly stable porous polymeric networks, as shown by Fang and co-workers [94]. On the other hand, Coskun and co-workers showed the preparation of microporous polymers from catalyst and solvent free polymerization process that enables direct utilization of elemental sulfur for the synthesis of BTAPs with BET surface areas up to 750 $m^2 g^{-1}$ [95]. To synthesize the BTAPs polymers, *p*-tolyl and 4-aminophenyl moieties are heated with elemental sulfur at 275 °C under Ar atmosphere. The as-prepared BTAPs were then heated at 400 °C to remove excess sulfur and activate the pores, thus eliminating the post-washing step. BTAPs showed excellent CO_2 separation performance under flue gas, natural gas, and landfill gas conditions. Hence, the use of low-value sulfur for repeatedly synthesis of BTAPs, is useful for large-scale application. Additionally, the targeted polymers should contain narrow pore size distribution, small pore width (≤6 Å) and smaller size (20–30 nm), for increasing selectivity towards CO_2 adsorption. Although several polymerization routes [89] have accomplished the criteria by developing different functional polymers, however it will be also interesting to discuss the effect of different polymerization pathways to introduce same functional polymer. For this reason, Buyukcakir et al. [96] explored the merits of different polymerization routes on the gas adsorption properties of same azobenzene polymers (NABs). The authors showed that the effect of N_2-phobic environment in these azo polymers is different because of their variation in particle size (20–500 nm), pore size (0.52–0.71 nm) and the uniformity of narrow pores, which ultimately give different CO_2/N_2 selectivity (37–64) at 0 °C and (26–96) 25 °C.

2.2.1.3. High surface area non-nitrogenous POPs as CO_2 adsorbent. Among several non-nitrogenous POPs, ultrahigh surface area PAF-1 is important, formed *via* Yamamoto homocoupling of tetrahedral monomers (tetrakis(4-bromophenyl)methane) as developed by T. Ben et al. [97] Owing to the in-build generation of diamondoid framework topology by the cross-linking of tetrahedral monomers, it creates open and interconnected pores having high specific surface area (BET: 5600 $m^2 g^{-1}$) and good CO_2 storage capacity (29.5 mmol g^{-1}, 298 K, 40 bar). Later, significant contribution has been made by modifying with other quadricovalent building centers, which form PPN-3 (with adamantine-system), PPN-4 (replaced tetrahedral carbon by silicon) and PPN-5 (replaced tetrahedral carbon by Germanium) [98], as shown in Fig. 10. Importantly, all these POPs have exceptionally high surface area. It is to be noted that PPN-4 having BET surface area of 6461 $m^2 g^{-1}$ considers as highest surface area POP among all the reported POPs till date. The exceptionally high surface area enables PPN-4 with excellent CO_2 storage capacity (48.2 mmol g^{-1}) at 50 bar and 22 °C. Therefore, it can be arguably said that the design and synthesis of high surface area POPs from tetrahedral building block is a promising approach for CO_2 storage at high pressure. Another class of POPs enriched with oxygen containing functional sites, is known as hypercrosslinked polymers (HCPs). Due to the availability of polar oxygen sites, HCP demonstrates a strong dipole-quadruple interaction with CO_2 for its storage and conversion purposes. HCPs exhibit unique property in gas storage capacity due to their highly cross-linked network which prevents the interconnected porous frameworks from being collapsed [99]. In Fig. 11, the formation of cross-linked HCP is shown. The synthesis of HCPs is advantageous in materials chemistry since it requires low-cost and abundant chemicals and catalysts.

Through knitting polymerization approach, several aromatic polymers can be easily prepared as described by Cooper and co-workers [100]. They demonstrated that high BET (1015 $m^2 g^{-1}$) polymers can be formed from the knitting polymerization of 1,1′-binapthol (4), which are helpful towards large CO_2 adsorption (3.96 mmol g^{-1}, 1 bar) and better CO_2/N_2 selectivity (26). These results substantiate that HCPs are also useful for carbon capture purposes. Interestingly, these HCPs could adsorb large CO_2 only at dry conditions and fail in moist condition, indicating these materials might not be suitable for CO_2 separation in humid condition. It is worthy to mention that HCPs are predominately non-conjugated in nature; however, considering the synthesis condition of HCP, parallel Scholl reaction can also take place depending on the substrate. As a result, the synthesized HCPs are partially conjugated instead of complete non-conjugated structure, as shown by Modak et al. [101] and they described three types of HCP materials (conjugated, non-conjugated, partially conjugated) starting from spirobifluorene as precursor.

The advantage of using spirobifluorene is huge because spirobifluorene molecule is rigid and consists of two biphenyl rings being connected through a tetrahedral node that constitutes stable & interconnected void spaces in POP. These spirobifluorene materials like COP-3, COP-3-rt and COP-3C (Fig. 12) possess high specific surface area of 1980, 1490 and 940 $m^2 g^{-1}$ respectively together with CO_2 uptake capacity as high as 4.6, 3.5 and 2.1 mmol g^{-1} respectively at 0 °C and 1 atm pressure. This study clearly justifies the advantage of oxygen-rich hypercrosslinked networks (COP-3, COP-3-rt) for adsorption of high CO_2 than conjugated COP-3, because non-conjugated HCP shows extra advantage of having polar oxygenated functional sites. Therefore, the addition of linker dimethoxymethane during the synthesis of HCPs is highly desirable in making alkoxy rich functional polymers.

Another interesting research has been done by Puthiaraj et al. [102] where the knitting polymerization has also been utilized for binding tetraphenyl aromatic moieties. Unlike the conventional Suzuki/Sonogashira coupling reactions, HCP polymerization promotes the cross-linking between tetrahedral aromatic moieties in a facile way. In continuation to this research, silicon and germanium containing nanoscale hypercrosslinked aromatic polymers (PHAPs) were reported using $FeCl_3$ mediated Friedel – Crafts alkylation between tetraphenylsilane or tetraphenylgermanium as a building block and formaldehyde dimethylacetal as a cross-linker, producing high surface area (1137-1059 $m^2 g^{-1}$) stable polymers having high CO_2 adsorption capacity (104.3–114.4 mg g^{-1}) with an isosteric heat of adsorption in the range of 26.5–27.3 kJ mol^{-1}. It can be said that controlled synthesis of silicon and germanium-based nanoscale POPs possess much difficulty in other polymerization route, but can easily be prepared from knitting techniques. In contrary, Han's group [103] reported three hydroxyl containing POPs (PFPOP-1-3; Fig. 13) through the utilization of phenol-formaldehyde resign chemistry, which, by virtue of having abundant hydroxyl groups and inherent microporosity, are suitable for carbon

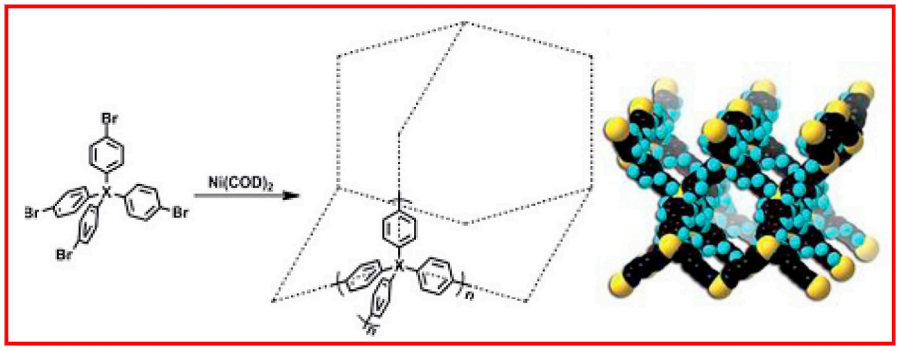

Fig. 10. Synthetic routes for high surface area PPN-3 (X: adamantane), PPN-4 (X: Si), PPN-5 (X: Ge), PAF-1 (X: C) from tetrahedral building blocks; Molecular modeling of non-interpenetrated diamondoid network of PPN-4 (black, C; pale grey, H; grey, Si) has been shown, written with permission from Ref. [98].

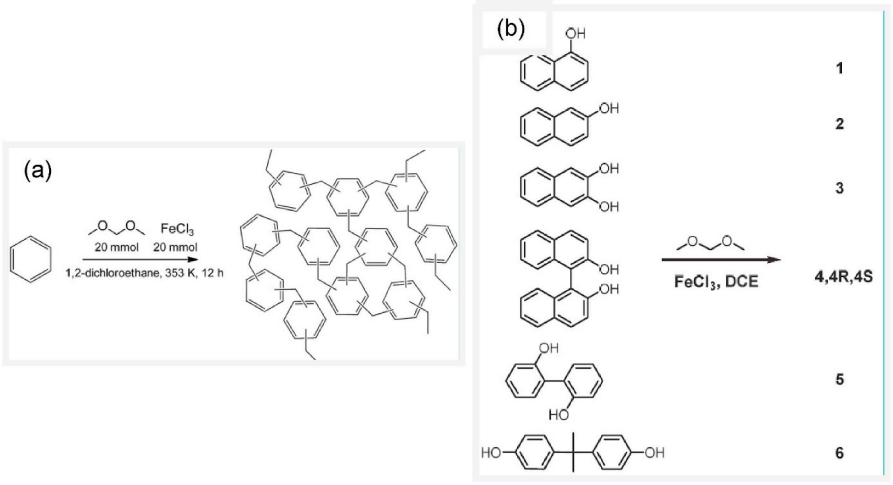

Fig. 11. (a) Synthesis of HCP from benzene as only precursor and (b) HCPs synthesized from various organic precursors, reproduced with permission from Ref. [100].

storage purposes. These PFPOPs have moderate BET surface area of 570, 630 and 530 $m^2 g^{-1}$ for PFPOP-1, PFPOP-2 and PFPOP-3 respectively and among them, PFPOP-3 has the highest CO_2 storage capacity of 4.74 mmol g^{-1} at 0 °C and 1 bar pressure. Meanwhile, PFPOPs exhibit considerable selectivity of CO_2 over N_2 (43.7–56.5) when calculated using ideal adsorption solution theory (IAST) and considering flue gas mixtures (CO_2/N_2 = 15/85) at 0 °C and 1.0 bar pressure.

2.2.1.4. POPs with N, S as heteroatoms. Although high BET surface area and oxygenated sites are necessary for influencing CO_2 adsorption, additionally N, S and B as heteroatom are also equally important for enhancing CO_2 selectivity at both high and/or low pressure due to adsorbent/CO_2 interaction. To demonstrate the effect of heteroatoms, several researches have integrated the POP frameworks with porphyrin, imine, carbazole, azo, benzimidazole, melamine, pyridine as nitrogen

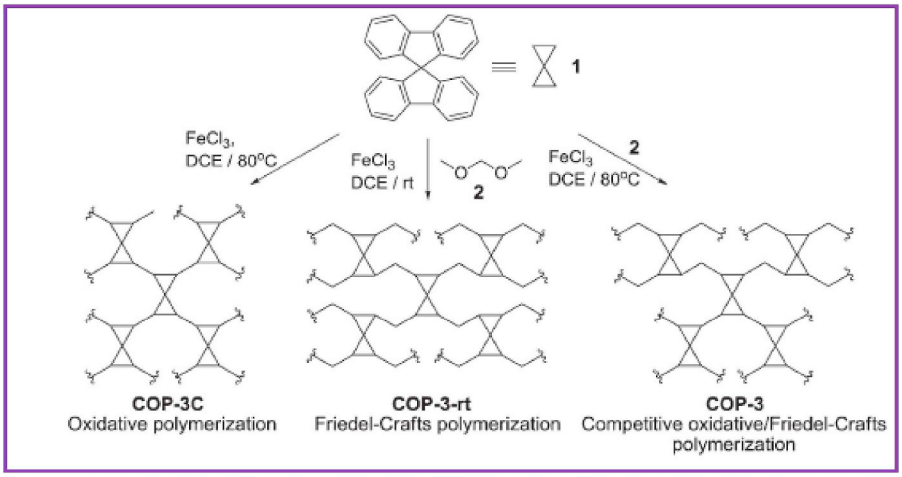

Fig. 12. Synthesis of spirobifluorene-based conjugated microporous polymers, COP-3C, COP-3-rt and COP-3 by $FeCl_3$ mediated polymerization reaction, reproduced with permission from Ref. [101].

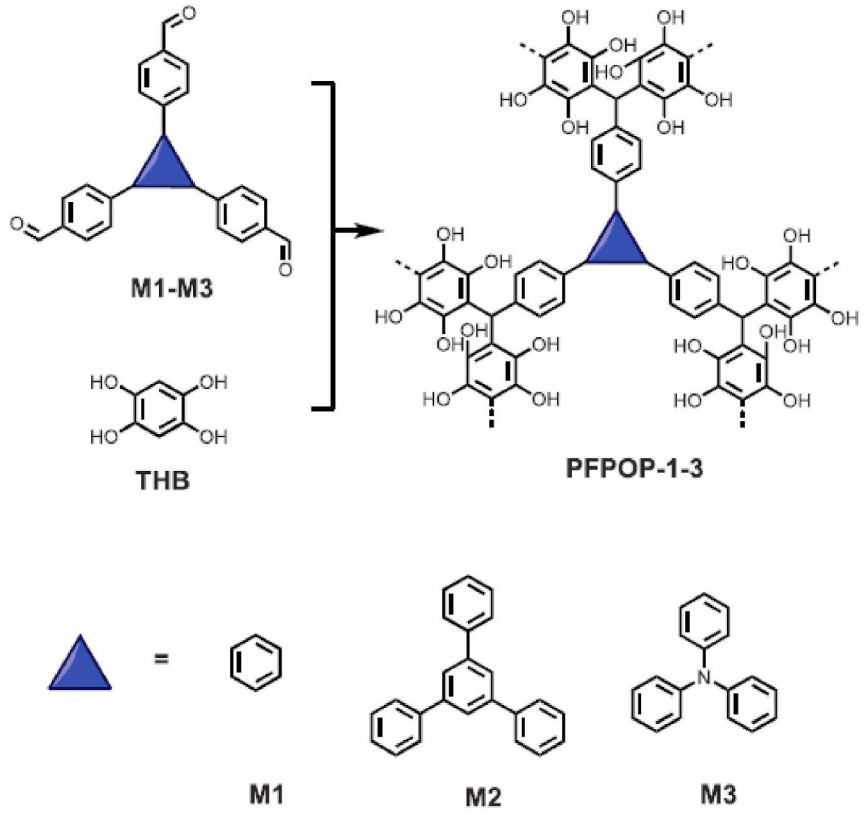

Fig. 13. Synthesis of PFPOP-1, PFPOP-2, and PFPOP-3, taken with permission from Ref. [103].

containing sites and thiophene as sulfur containing sites to improve their isosteric heat of adsorption with CO_2. As for instance, pyridine and thiophene containing POPs *e.g.;* PON-2 and PON-3 show CO_2 uptake capacity of 10.9 and 11.9 mmol g^{-1} respectively at −78 °C and 1 atm pressure, in spite of their poor BET surface area of 168 (PON-2) and 51 $m^2 g^{-1}$ (PON-3). Under similar condition, PON-1 exhibits 22.2 mmol g^{-1} CO_2 adsorption capacity, although the framework is devoid of any heteroatom and possesses 1422 $m^2 g^{-1}$ BET surface area [104]. This result signifies that although PON-2 and PON-3 are non-porous but they show high CO_2 capture, probably due to the smaller kinetic diameter of CO_2 (3.3 Å) than that of N_2 (3.64 Å), which facilitate small CO_2 molecules to easily access small pores than that of N_2 molecules. Alternatively, it can be said that although Pyridyl and thiophenyl moieties are not suitable for producing high surface area materials because of their low activity, but still their lone pair will appear to be critical in providing strong interaction with CO_2 through dipole-dipole. Moreover, at 25 °C and 1 bar, CO_2 uptake efficiency of PON-1 (2.5 mmol g^{-1}), PON-2 (0.7 mmol g^{-1}) and PON-3 (0.8 mmol g^{-1}) is interesting and the result of PON-1 might be comparable with the highest surface area materials PAF-1 (BET: 5600 $m^2 g^{-1}$) [97] and MOF-177 (BET: 4500 $m^2 g^{-1}$) [30], which undoubtedly augment the requirement of polar frameworks for capturing CO_2.

2.2.1.4.1. Carbazole functionalized POP. Carbazole-based POPs (CPOP-1) were prepared by Chen et al. [105] through one-pot oxidative polymerization of carbazole with $FeCl_3$ as catalyst as shown in Fig. 14. CPOP-1 shows high BET surface area (2220 $m^2 g^{-1}$) and narrow pore size (0.62 nm). The presence of electron-rich carbazole unit facilitates prompting uptake of polarizable CO_2 molecule through local dipole-quadrupole interactions. The CO_2 uptake of CPOP-1 is as high as 4.8 mmol g^{-1} at 0 °C and 1 bar, along with its high selectivity for CO_2/CH_4 (33.0) and CO_2/N_2 (25.0) separation is also noticeable. They have also prepared CPOP-(2–7) [106] through this reaction and among several CPOPs, CPOP-7 exhibits the best CO_2 uptake capacity (3 mmol g^{-1} at 0 °C and 1 bar).

2.2.1.4.2. Triazine functionalized POP. Incorporation of electron withdrawing triazine unit in POP structure has many advantageous applications in material science [107,108]. Initiallly, triazine-linked POPs (CTFs) were prepared by Thomas and co-workers [109] through ionothermal polymerization of organic nitriles at very high temperature (~400 °C) in presence of $ZnCl_2$ catalyst, which acts as Lewis acid as well as solvents. Ordered microporous CTFs thus obtained possess high BET surface area (1235 $m^2 g^{-1}$) and excellent CO_2 uptake capacity (4.2 mmol g^{-1} at 1 atm, 0 °C). Again, several PCTFs were also synthesized through the modifications of CTFs using branched arms precursor [110]. Importantly, PCTF-1 with biphenyl, PCTF-2 with terphenyl and PCTF-3 with quaterphenyl rings have been synthesized and have BET surface area of 853, 811 and 395 $m^2 g^{-1}$ respectively. When the middle benzene ring of CTF has been replaced by the strong polar group, such as benzothiadiazole, it forms PCTF-4 which shows highest CO_2 uptake of 4.7 mmol g^{-1} at 0 °C and 1 bar. Wang et al. [111] reported two covalent triazine-based frameworks (CTFs) with ultramicropores (< 7 Å) based on short (fumaronitrile, FUM) and wide monomers (1,4-dicyanonaphthalene, DCN). The obtained CTF-FUM and CTF-DCN show excellent stability, combined with outstanding ability to selectively capture CO_2 due to ultramicroporous nature. Especially, CTF-FUM-350 has the highest nitrogen content (27.64%) and thus it has large CO_2 adsorption capacity (2.56 mmol g^{-1} at 25 °C) and selectivity for CO_2 over N_2 and CH_4 (102.4 and 20.5 at 25 °C respectively). The authors claimed that CO_2/CH_4 separation selectivity

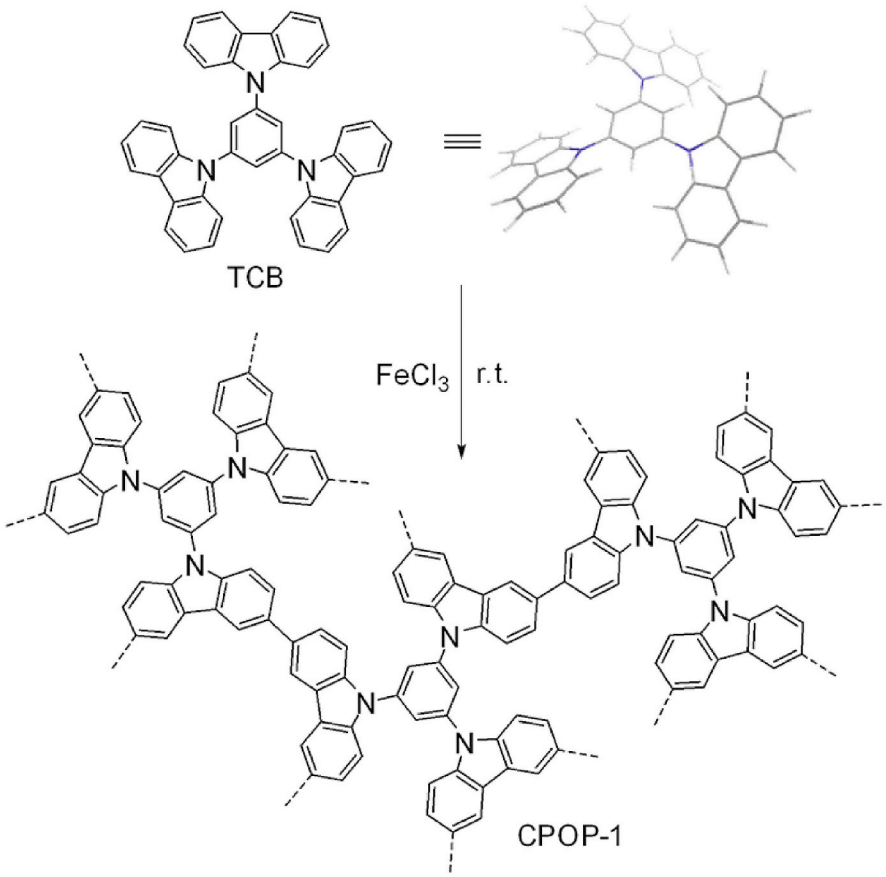

Fig. 14. Syntheses route to microporous polycarbazole CPOP-1, taken with permission from Ref. [105].

is larger than that of all the reported CTFs and ranks in top 10 among all reported POFs.

On the other hand, Cooper group [112] reported a series of conjugated microporous polymers based on electron-withdrawing 1,3,5-triazine linkage (TCMPs) by palladium-catalyzed Sonogashira-Hagihara cross-coupling reaction. Although the surface area of TCMP was similar to the corresponding benzene-based CMPs, the CO_2 uptake capacity was higher for TCMPs. In particular, TNCMP-2 exhibited high surface area ($995\ m^2\ g^{-1}$) and efficient CO_2 uptake ($1.45\ mmol\ g^{-1}$) at 25 °C and 1 bar. Furthermore, Zhu and co-workers [113] reported the synthesis of porous aromatic framework PAF-56P *via* cross-coupling of cyanuric chloride and *p*-terphenyl monomers (Fig. 15). PAF-56P exhibits a three dimensional framework with a large pore size of 12 Å and high CO_2 uptake ($1.52\ mmol\ g^{-1}$) at 25 °C and 1 bar.

2.2.1.4.3. Porphyrin functionalized POPs. Porphyrin containing microporous POPs were generally reported from expensive Pd and Ni catalyst [114,115], however Modak et al. [116,117] introduced a new method to make porphyrin polymers from one-pot bottom up approach considering electrophilic aromatic substitution between pyrrole and linear dialdehydes in presence of small amount of $FeCl_3$ as catalyst (Fig. 16). By increasing the length of phenyl linkers, Fe-POP-1/2/3 materials were formed having BET surface area of 875, 855 and $750\ m^2\ g^{-1}$ respectively. Owing to strong Van der Waals interaction between porphyrin and CO_2 sites, Fe-POP exhibits CO_2 uptake of about $4.3\ mmol\ g^{-1}$ at 0 °C, 1 atm). Importantly, Fe-POP contains low loading of iron ($0.003\ mmol\ g^{-1}$), signifying that framework-CO_2 interaction is

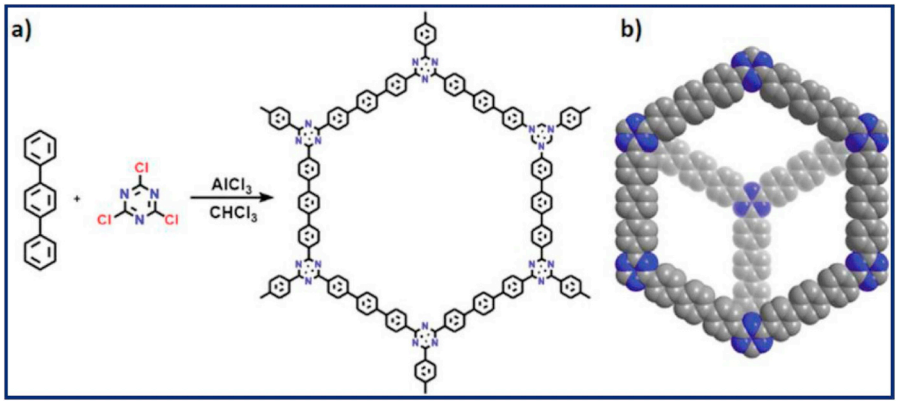

Fig. 15. (a) Synthesis of PAF-56P and (b) Stacked structure of PAF-56P drawn by materials studio; taken with permission from Ref. [113].

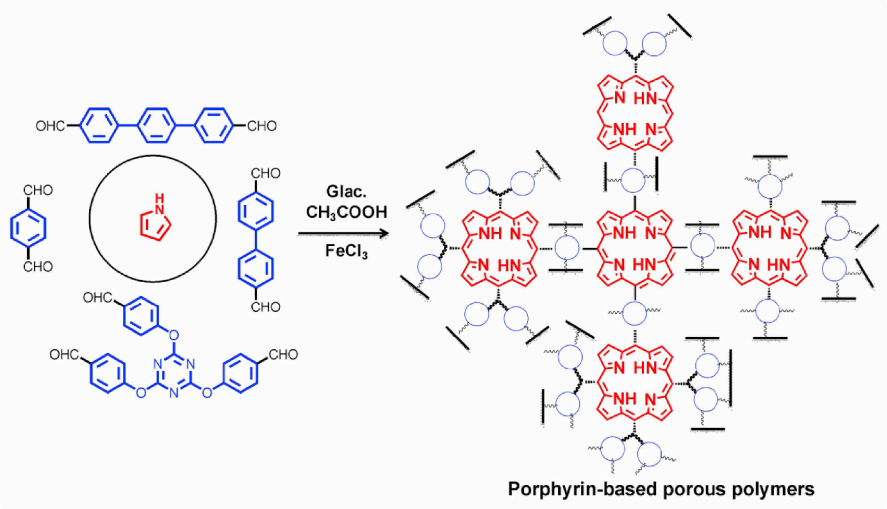

Fig. 16. Schematic representation for the preparation of porphyrin-based porous polymers by electrophilic substitution of pyrrole with several aromatic aldehydes.

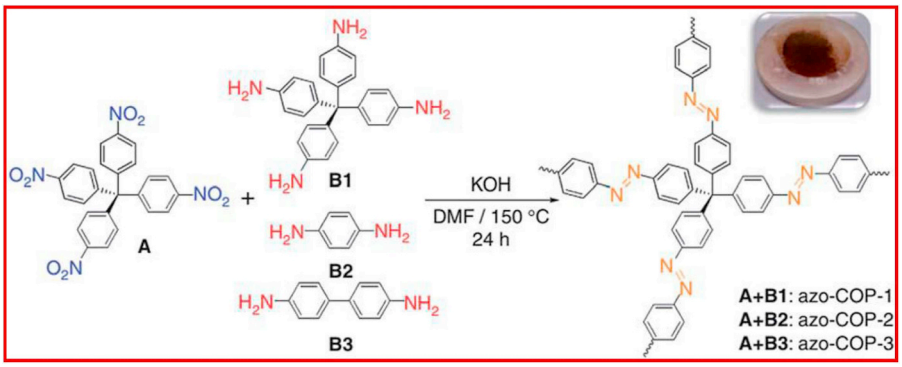

Fig. 17. Synthesis of Azo-POP, reproduced with permission from Ref. [118].

responsible for enhanced CO_2 adsorption. Later, this research has been extended by changing aromatic dialdehydes to aromatic trialdehyde and using 4,4′,4″-(1,3,5-triazine-2,4,6-triyl)tris(oxy)tribenzaldehyde as tripodal precursor. The advantage of using this organic precursor is enormous, because it introduces both triazine and porphyrin networks in a single TPOP-1 material, resulting high uptake of CO_2 (6.2 mmol g^{-1} at 3 bar, 0 °C) [117].

2.2.1.4.4. Azo-based POPs. Nanoporous azo-COPs were reported by Patel et al. [118] by catalyst free coupling of aromatic nitro and amine moieties under basic conditions (Fig. 17), having 729 $m^2 g^{-1}$ of BET surface area and 2.5 mmol g^{-1} of CO_2 uptake capacity at 0 °C and 1 bar. On the whole, high CO_2 uptake capacity of 3.4 mmol g^{-1} at −10 °C and 1 bar is noticed with these frameworks. Interestingly, the azo group makes the frameworks repellent to N_2, exhibiting high selectivity in CO_2/N_2 separation at high temperature. Thus, with the incorporation of azo moiety, POPs can serve as good candidate for highly selective gas separation purposes. In order to explain, the authors have done a Monte Carlo simulation for understanding high CO_2/N_2 selectivity of these frameworks. Based on the theoretical analysis they showed that although N_2 adsorption is enthalpically favorable, the entropy loss upon binding of N_2 molecules causes N_2 phobicity of azo groups. This work represents the importance of azo groups in separation of CO_2 and N_2 mixtures, which is furthermore promising for post-combustion CO_2 separation. Accordingly, Arab et al. [119] prepared azo-based polymers (ALPs) by a facile homo coupling reactions of aniline-like building units with copper (I) bromide as catalyst. Among several ALPs, ALP-1 shows high BET surface area of 1235 $m^2 g^{-1}$ and high thermal and chemical stability. In addition, ALP-1 exhibits a significant CO_2 uptake capacity (5.36 mmol g^{-1}) at 0 °C and 1 bar. It is worth mentioning that large CO_2 uptake selectivity with these N_2-phobic azo-polymers are basically as a result of dipole-dipole interaction between electron rich azo units and Lewis acidic CO_2.

2.2.1.4.5. Triazole-based POPs. Generally azide and alkynyl moieties can undergo a Cu(II) catalyzed click cycloaddition reaction in order to make Triazole-linked structures. Based on this reaction, triazole-based POPs are usually synthesized. Cooper and co-workers [120] reported polytriazole as robust framework obtained from tetrahedral monomers (Fig. 18). Although the surface area of this network is not high, but at 298 K and 1 bar, it exhibits high CO_2 uptake (2.20 mmol g^{-1}), which is most likely because of electron-rich triazole unit in the network. Also, this network exhibits highest heat of adsorption (33.7 kJ mol^{-1}) at low CO_2 coverage compared to the other networks for post-combustion carbon capture.

2.2.1.5. Nanotube/nanoflower shaped POPs as CO_2 adsorbent. While most POPs are reported as agglomerated solid spheres, very few shows interesting hollow spheres or tubular morphology. Considering the increasing impact of hollow particles in materials science, it is greatly evident that POPs with in-build micropores together with large hollow mesopores have distinct advantages in gas adsorption and catalysis [121,122]. Remarkably micropore favors specific molecular-level interaction and large mesopore could allow enhanced mass transportation or efficient diffusion. Therefore, the combination of both micropores and large mesopores in HOPs are quite unique. In

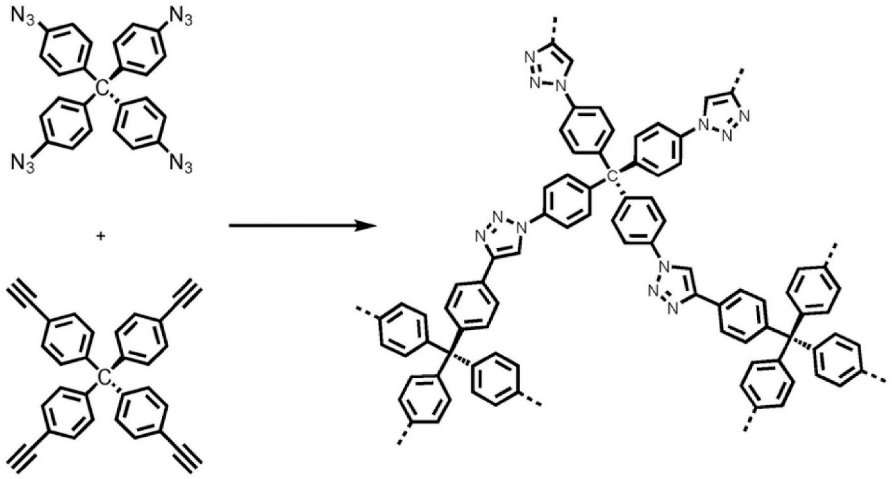

Fig. 18. Synthesis of triazole-based POP, taken with permission from Ref. [120].

literature, there are some reports on POP based hollow nanotubes/hollow spheres, obtained from Sonogashira/Glaser type coupling reactions without or with SiO_2 as hard template in presence of expensive precursors, costly catalysts and long reaction process [121,123]. However, Modak et al. showed a convenient and mild protocol to synthesize amine functionalized hypercrosslinked hollow tubes [85] through $FeCl_3$ mediated polymerization of 4-tritylaniline with dimethoxymethane (DMM) at 80 °C (Fig. 19). The authors prepared several POP nanotubes with BET surface area of 660-530 $m^2 g^{-1}$ and CO_2 uptake capacity between 2.7 and 2.2 mmol g^{-1} by varying DMM concentration during the synthesis. Their investigation is suggesting carbon capture property by free amine containing porous polymer tubes.

Another non-functionalized poly(aryleneethynylene)-based POP nanotubes (CMPN-1,2,3) were reported by Deng and co-workers [124] having BET surface area as calculated to be 230 $m^2 g^{-1}$ for CMPN-1, 339 $m^2 g^{-1}$ for CMPN-2 and 1368 $m^2 g^{-1}$ for CMPN-3. Despite their high BET, they show moderate CO_2 uptake efficiency at 0 °C and 1 bar pressure, where CMPN-1, CMPN-2 and CMPN-3 demonstrate CO_2 uptake of 0.9, 1.7, 0.9 mmol g^{-1} respectively, which are certainly lower than amine/alkoxy functionalized PP-1,2,3 prepared by Modak et al. [85]. Therefore, it can be arguably said that nanotubes with suitably decorated functional sites would be interesting as CO_2 scavenger. Apart from nanotubes, nanoflower-shaped POPs [125] are also interesting as CO_2 adsorbent (Fig. 20). As for example, a triazine-piperazine based 3D nanoflower polymer (CTPP) containing abundant Lewis basic sites

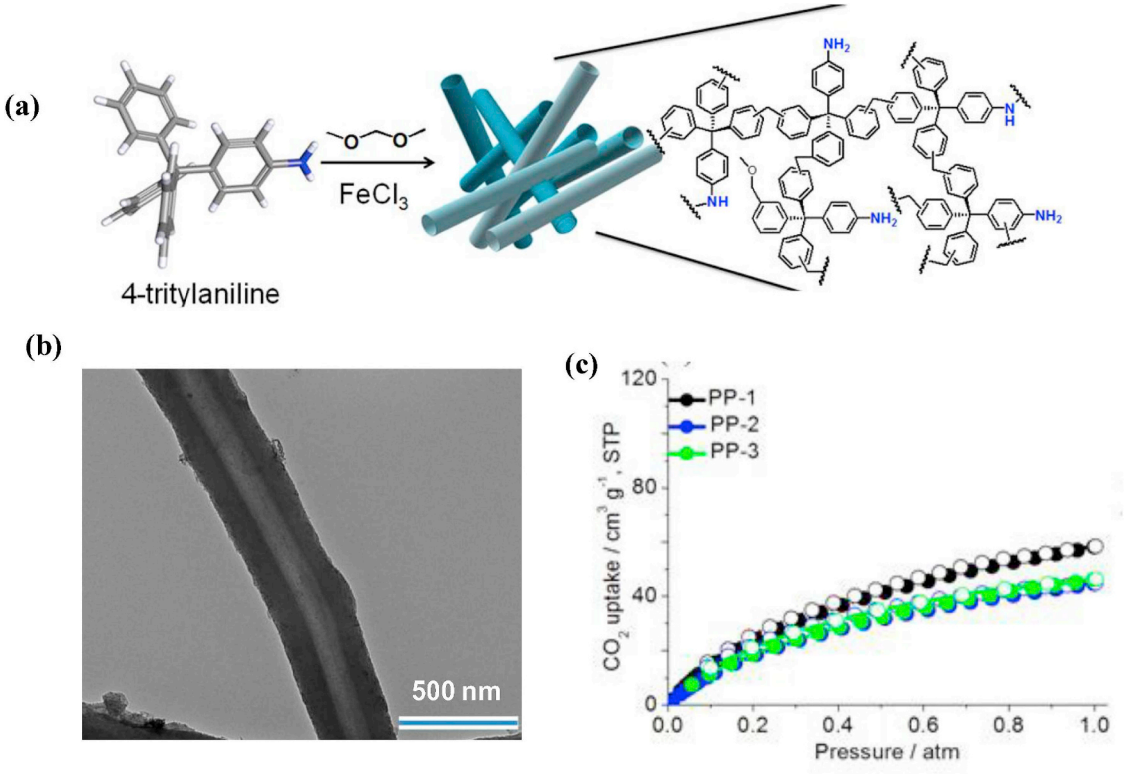

Fig. 19. (a) Schematic representation for the synthesis of POP-nanotubes; (b) TEM image of PP-3; (c) CO_2 sorption isotherm of PP-1,2,3, taken with permission from Ref. [85].

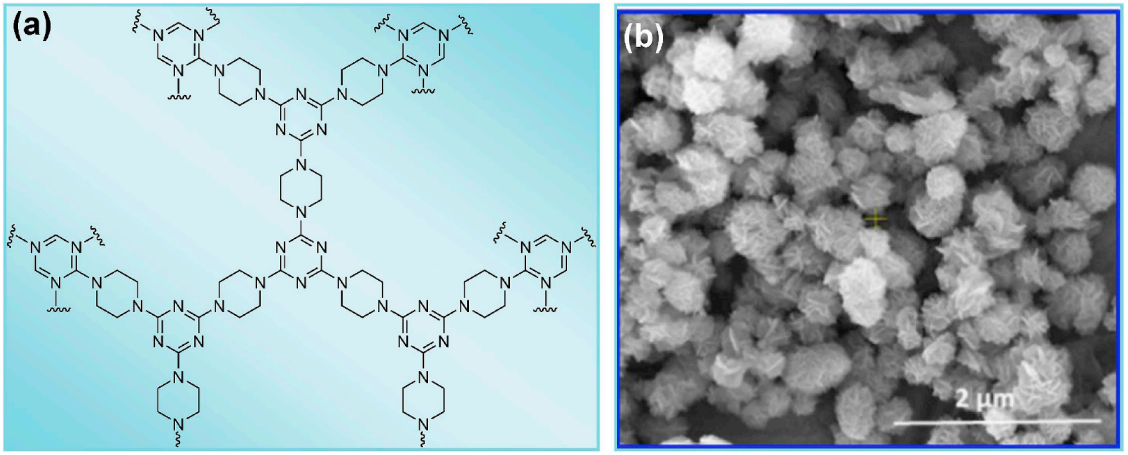

Fig. 20. (a) Nanoflower-shaped triazine containing polymer and (b) SEM image, taken with permission from Ref. [125].

possesses high surface area (779 $m^2 g^{-1}$) and corresponding high CO_2 uptake capacity (3.48 mmol g^{-1}) at 0 °C and 1 bar, along with high CO_2/N_2 (128) separation selectivity and strong heat of adsorption (34 kJ mol^{-1}) for CO_2.

2.3. Covalent organic frameworks (COFs)

In addition to MOFs and amorphous POPs, COFs attracted significant attention in recent years as an ideal adsorbent towards carbon capture [126]. Ever since the discovery of COFs in 2005 by Yaghi and co-workers [127], they show significant merit as promising CO_2 adsorbents as they have ordered pore distribution, low energy requirement for regeneration, good stability, easy pore surface engineering, high structural diversity and rich in porosity. The inherent advantage of COFs is their low framework density, which is suitable for gas storage and transportation purposes. COFs are prepared from organic monomers through the reticular chemistry approach, which make COFs highly robust and stable even under drastic condition. Unlike POPs which are synthesized from fast reaction kinetics, formation of crystalline COFs required slow and reversible condensation reactions through B-O (in boroxine, boronate), C=N (in imines, hydrazine, squaraine) and N-N (in azodioxides) bond formation reactions.

It is worth mentioning that COFs have close similarity with POPs in synthesis mechanism, easy fabrication as thin film, tailorable chemical structure as well as easy functionalization etc. Hence, it can be said that despite enormous development in the synthesis and applications, few reports only concentrate COFs as CO_2 adsorbent [126]. Thus, it is highly demanding to highlight the progress of recent COFs as post-combustion CO_2 capture materials and also to understand the limitations of these materials. In this review, we have summarized important COFs having excellent efficiency towards CO_2 adsorption.

2.3.1. COFs having B-O linkages

In 2005, Yaghi and co-workers first discovered B-O bond based COFs containing six or five membered boroxine (B_2O_3; using 1,4-benzene diboronic acid (BDBA) precursors) and/or boronate (C_2O_2B; using BDBA and HHTP) rings that form COF-1 and COF-5 respectively having two-dimensional (2D) architectures [127]. Later in 2008–2009, they were explored as efficient gas adsorbing materials, particularly for CO_2 [128]. Another type of COF; namely COF-6 {synthesized by BTBA and HHTP}, COF-8 (BTPB

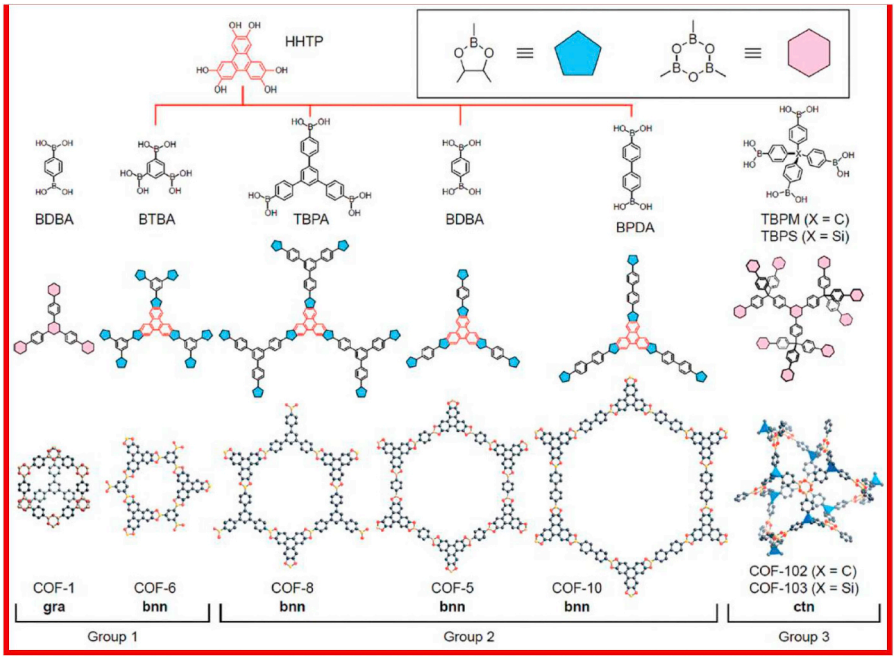

Fig. 21. Condensation reactions of boronic acids and HHTP used to produce COFs (upper row), and resulting in fragments of COFs (middle row). Atomic connectivity and structures of crystalline 2D and 3D COFs (last row). The topology and the group classification number are indicated for each COF, taken with permission from Ref. [128].

and HHTP), and COF-10 (BPBA and HHTP) were explored later through reticular chemistry approach [129]. Except COF-1 with staggered conformation, all these 2D COFs show eclipsed layered conformation in *bnn* net. In 2007, COFs with 3D structure were prepared using triangular and tetrahedral nodes *via* targeting *ctn* and *bor* nets, which include the synthesis of COF-102 and COF-103 solids respectively. COF-102 and COF-103 were prepared by self-condensation reaction of tetrahedral tetraboronic acid TBPM and TBPS respectively, exhibiting boroxine ring containing 3D *ctn* networks, as shown in Fig. 21 [130]. Ar adsorption isotherm of COFs follows the sequence of BET surface area, COF-102 (3620-3530 $m^2 g^{-1}$) > COF-10 (1760 $m^2 g^{-1}$) > COF-5 (1670 $m^2 g^{-1}$) > COF-8 (1350 $m^2 g^{-1}$) > COF-1 and COF-6 (750 $m^2 g^{-1}$). When considering CO_2 adsorption at low pressure (1 bar) and at 0 °C, the authors showed that these COFs exhibit the following order: COF-6 > COF-1 > COF-102 > COF-8 > COF-5 > COF-10, substantiating that CO_2 uptake is not dependent on BET surface area or pore volume of these COFs. Studies suggests that pore width is imperative in this case as COF-6 having lowest surface area in these series, but shows smallest pore size (0.9 nm) for maximum CO_2 uptake. However, at high pressure (1–55 bar) condition, CO_2 uptake follows the reverse order: COF-102 (611 $cm^3 g^{-1}$) > COF-103 (606 $cm^3 g^{-1}$) > COF-10 (514 $cm^3 g^{-1}$) > COF-5 (443 $cm^3 g^{-1}$) > COF-8 (321 $cm^3 g^{-1}$) > COF-6 (158 $cm^3 g^{-1}$) > COF-1 (117 $cm^3 g^{-1}$) in accordance to the BET surface area [128–131].

Additionally, mesoporous COF, namely TDCOF-5 was also prepared from 1,4-benzenediboronic acid and hexahydroxytriptycene by Kahveci at al.[132]. Although TDCOF-5 exhibits high BET surface area (2497 $m^2 g^{-1}$) and well mesoporosity (2.6 nm), it has lower CO_2 uptake ability (2.09 mmol g^{-1}) at 0 °C and 1 bar pressure than other adsorbents, implying that mesoporous COFs with wide pore size are not suitable for low pressure CO_2 capture. Although B-O linked COFs have good crystallinity, large BET and considerably high thermal stability, they possess low CO_2 uptake property at low pressure. Furthermore B-O linking in COFs is not suitable for exhibiting high water tolerability, which limits their practical application for CO_2 storage. Hence, post modification could be the only way to solve low CO_2 storage criteria.

2.3.2. COFs with imine sites

Using dynamic covalent chemistry approach, Uribe-Romo et al. [133] have developed imine-condensation reactions in order to make crystalline COF materials. In 2009, the first 3D COF, COF-300 was prepared from “Schiff base” condensation between aldehyde and amine in the presence of acetic acid solution, which was later extended with hydrazine instead of branched aromatic amines for the formation of hydrazine COF [134]. Subsequently, COFs are being utilized as CO_2 adsorbents by several researchers.

In 2012, Banerjee and co-workers [135] have developed some interesting 2D COFs (TpPa-1 and TpPa-2) from 1,3,5-triformylphloroglucinol (Tp) with p-phenylenediamine (Pa-1) and 2,5-dimethyl-*p*-phenylenediamine (Pa-2) respectively. It is worth mentioning that the application of pholoroglucinol derivatives in making COF framework is attracting due to its ability of reversible tautomerism from the enol-imine (OH) to the keto-enamine form, which could impart additional stability to these COFs in strong acid as well as in strong basic conditions. It is pertinent to mention that phloroglucinol derivatives have huge prospects in materials science for designing highly functional materials [136–138].

Notably, TpPa-1 and TpPa-2 materials are predominately microporous (1.25 nm pore size) with high BET surface area (535 $m^2 g^{-1}$) and shows CO_2 uptake capacity of about 78 and 64 $cm^3 g^{-1}$ respectively at 0 °C and 1 bar. Similarly, several COF materials were prepared using different diamine building blocks as benzidine (BD) [139]. Thus, TpBD COFs [139] can be synthesized at room temperature from solvent-free mechanochemical way and investigated for CO_2 adsorption purposes. As for example, TpBD shows CO_2 uptake efficiency of about 2 mmol g^{-1}, while 3.5 and 2.8 mmol g^{-1} are observed for TpPa-1 and TpPa-2 at 0 °C and 1 atm pressure. In order to improve the structural stability of COF frameworks, they prepared hydroquinone functionalized COF, which remains near to C=N group [140]. Because the hydroquinone sites with free –OH groups can make intermolecular hydrogen bonding with imine sites that could be effective in protecting COF interior for damaging the COFs structure. These H-bonded COFs are named as DhaTph and DmaTph, having high surface area of 1305 (DhaTph) and 431 $m^2 g^{-1}$ (DmaTph) respectively. These COFs exhibits moderate CO_2 uptake property (DhaTph; 2.9 mmol g^{-1}; DmaTph; 1.6 mmol g^{-1}).

On the other hand, N-rich COFs are better candidate as CO_2 adsorbents [141]. El-Kaderi and co-workers synthesized mesoporous imine linked COF (ILCOF-1) [142] with high surface area (2723 $m^2 g^{-1}$) by the condensation reaction between 1,3,6,8-tetrakis (4′-formylphenyl)-pyrene and *p*-phenylenediamine in 1,4-dioxane in the presence of aqueous acetic acid at 120 °C over 3 days. Schematic representation for the solvothermal synthesis of COF by imine condensation reaction has been presented in Fig. 22. Although ILCOF-1 exhibits moderate CO_2 uptake at low pressure (1.4 mmol g^{-1} CO_2 at 0 °C, with a Q_{st} value of 18.3 kJ mol^{-1}), but higher CO_2 uptake (29.3 mmol g^{-1}) is seen at 40 bar and 25 °C, which is quite higher than other 2D/3D COFs. This study clearly demonstrates the effect of N-functionalized ordered pore wall in COFs, which are better candidates than unfunctionalized COFs for CO_2 uptake.

2.3.3. Bifunctional COFs having dual covalency

All the previously reported COFs demonstrate the formation of single covalent bond having only one linkage *i.e.*; either B-O or C-N. However design and construction of new COFs with two/more types of covalent bond will surely widen the scope of advanced scientific research of porous materials. Zhao and colleagues [144] reported COFs with multiple covalent bonds through orthogonal reaction strategy, where not only binary COF (NTU-COF-1) is formed from the condensation between FPBA and TAPB, but also ternary COF (NTU-COF-2) having two types of covalent bonds is also formed. NTU-COF-2 showed type IV isotherm with 1619 $m^2 g^{-1}$ BET surface area and 2.5 nm of mesopores (Fig. 23). CO_2 adsorption measurement for NTU-COF-2 suggests that this material can store up to 2.3 mmol g^{-1} of CO_2 at 0 °C and 1.0 bar, with Q_{st} of 27.0 kJ mol^{-1} at low CO_2 coverage. In Fig. 24, we have presented several important COFs with different functionalities for CO_2 adsorption at low pressure and at 0 °C and 25 °C temperature. In Table 1, we have summarized CO_2 uptake capacity, selectivity and heat of adsorption of various amorphous and crystalline polymers.

Although COFs are an emerging class of porous crystalline materials and have wide scope of applications in the front-line areas, but they are yet to be commercialized. This drawback is because of the complex preparation process and the harsh solvothermal condition (sealed Pyrex tube, inert atmosphere and high pressure, non-reusable organic solvents etc). Hence, preparation of COFs under microwave, room temperature and under grinding condition could be far better for their future economical scale-up. Again, it could be competitive with other representative porous adsorbents, like MOFs and POPs. Additionally, processability is also an important factor for commercialization purpose. Therefore, apart from batch reactions, the synthesis of COFs through continuous flow system would be interesting for mass production of COFs owing to better reaction kinetics and high reaction yields. Hence, microfluidic [146] and surface patterning [147] techniques are two promising alternatives for COFs preparation, which are simple, easily processable and highly cost-efficient.

2.4. Porous oxide materials

In addition to MOFs, POPs or COFs, porous oxides are also quite promising for CO_2 capture. Unlike MOFs and POPs which have ultra-narrow micropores for CO_2 adsorption, mesoporous oxides possess wide pore aperture that might be insignificant as CO_2 adsorbent. However,

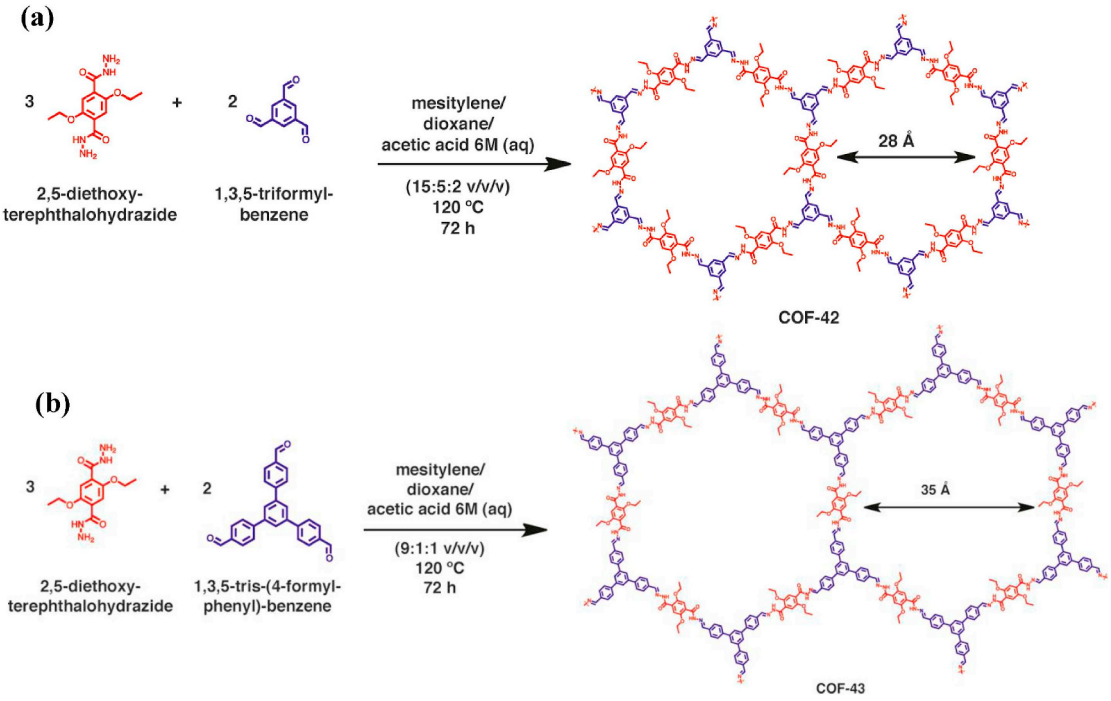

Fig. 22. Synthesis of (a) COF-42 and (b) COF-43 by Condensation of Linear 2,5 diethoxyterephthalohydrazide (red) with trigonal-planar 1,3,5-Triformylbenzene (blue) or 1,3,5-Tris(4-formylphenyl)benzene (blue) to make COF-42 and COF-43 (pore sizes are shown); taken with permission from Ref. [143]. (For interpretation of the references to color in this figure legend, the reader is referred to the Web version of this article.)

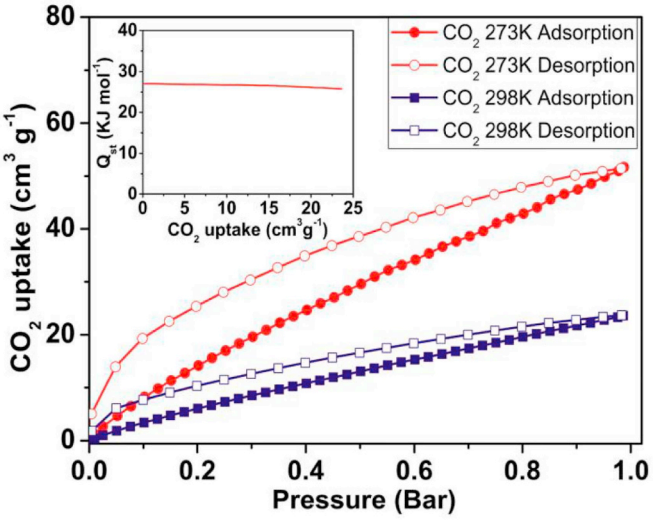

Fig. 23. CO_2 adsorption isotherms of NTU-COF-2. (Inset) Isosteric heat of CO_2 adsorption for NTU-COF-2, reproduced with permission from Ref. [144].

functionalization of oxides with CO_2-philic sites could enhance adsorption even from ambient air, i.e.; under ultra-dilute condition [148]. In order to meet the criteria, researchers developed several amine functionalized mesoporous oxides by co-condensation reaction between amine-based organosilica and mesoporous silica. The supported amines in silica framework can undergo chemical reaction with CO_2 through strong bond formation and allow significant CO_2 uptake even at low CO_2 pressure. It is worth noting that the heat of sorption and selectivity towards CO_2 are higher for chemisorption than that of physisorption, which are mainly determined from the amine loading on solid surface instead of their effective surface area. Notably, amine containing oxide supports are excellent candidates towards CO_2 storage under ambient air [149].

According to the synthesis condition, amine-based materials are of different types e.g.; (i) Class 1 materials which are prepared by impregnation of amines into the pores, (ii) Class II consisting of amines which are covalently bonded to the walls of porous materials and (iii) Class 3, where amine monomers are in-situ polymerized to polyamines inside the framework. In Fig. 25, we have given pictorial representation of all these classes of materials. To understand CO_2-amine interaction, Caplow and Danckwerts proposed that under anhydrous condition two

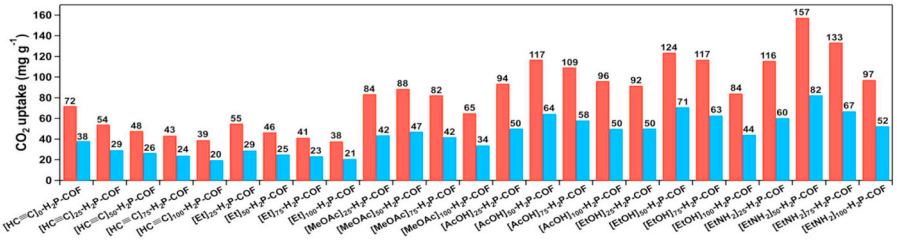

Fig. 24. CO_2 adsorption capacity of COFs at 273 (red) and 298 K (blue) at 1 bar, reproduced with permission from Ref. [145]. (For interpretation of the references to color in this figure legend, the reader is referred to the Web version of this article.)

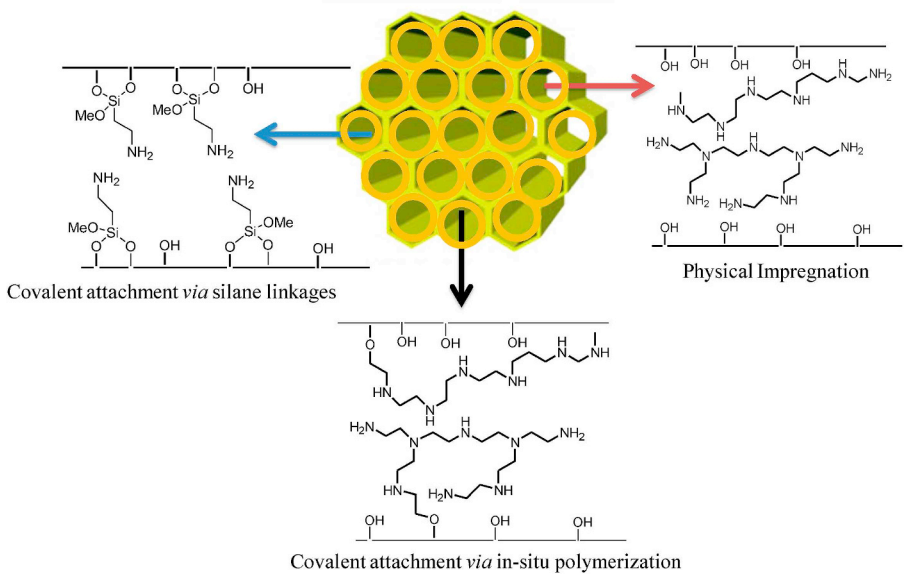

Fig. 25. Schematic representation of the formation of several amine-functionalized mesoporous silica.

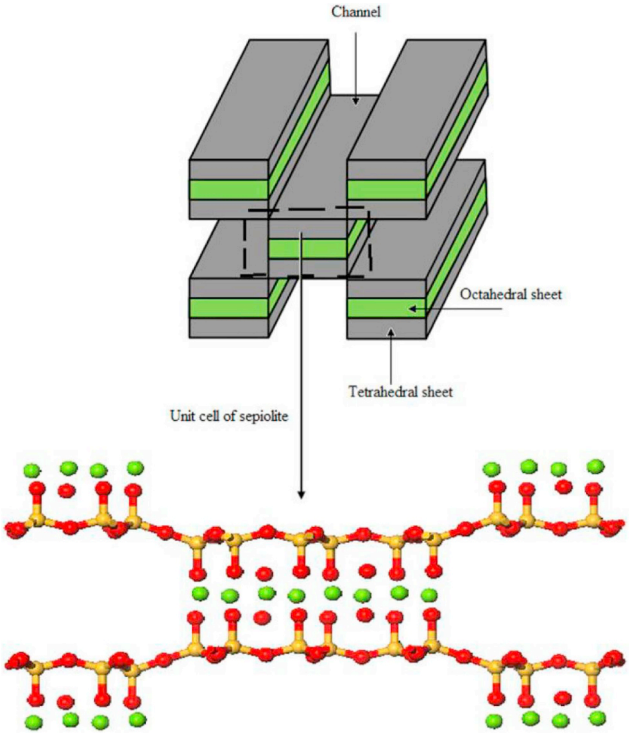

Fig. 26. Schematic representation of sepiolite structure, magnesium (green) octahedrally coordinated between chains of SiO_4 (silicon shown in yellow, oxygen in red), reproduced with permission from Ref. [157]. (For interpretation of the references to color in this figure legend, the reader is referred to the Web version of this article.)

amine molecules interact with one CO_2 molecule to form ammonium carbamate as adduct [150,151]. Based on this observation, maximum CO_2/N ratio that can be achievable is 0.5 mol CO_2/1 mol N. It is important to note that CO_2/N molar ratio is generally considered as amine efficiency. Again, they proposed that under humid atmosphere, CO_2 adsorption becomes double than that of anhydrous condition as ammonium carbonate or bicarbonate is produced, signifying better performance of amine-based mesoporous oxides in moist condition than in dry CO_2 atmosphere. This observation is slightly contradicting regarding CO_2 adsorption of hypercrosslinked polymers in moist condition [100].

Porous materials are advantageous owing to their flexible surface modification facility because of the availability of high surface area and lower regeneration energy compared to any conventional solvent based methods. Among the several porous materials, clay minerals are one of the significant materials due to their unique physical properties because of their layered structure, small grain size, and large surface to volume ratio. Furthermore, clay materials have high mechanical and chemical stability as well as low cost, as a result of which they have withdrawn specific attention to the researchers. Several clay minerals have shown their potentiality as an adsorbent for CO_2 uptake, e.g.; montmorillonite, halloysite, kaolinite, nanosepiolite, bentonite and so on. Using montmorillonite as support materials, W. Wang et al. [152] developed montmorillonite supported PEI composite for CO_2 capture, the CO_2 sorption efficacy was found to be 2.54 mmol g^{-1} under dry condition and 3.23 mmol g^{-1} under moisture added conditions. G. Rother et al. [153] performed neutron diffraction experiments on montmorillonite clay and measured the interlayer spacing and composition, which demonstrate that limited amounts of CO_2 was adsorbed into the interlayer region, leading to the depression of the interlayer peak intensity and an increase of the d(001) spacing by ~ 0.5 Å. They also verified that the density of CO_2 in the clay pores is comparatively stable over a wide

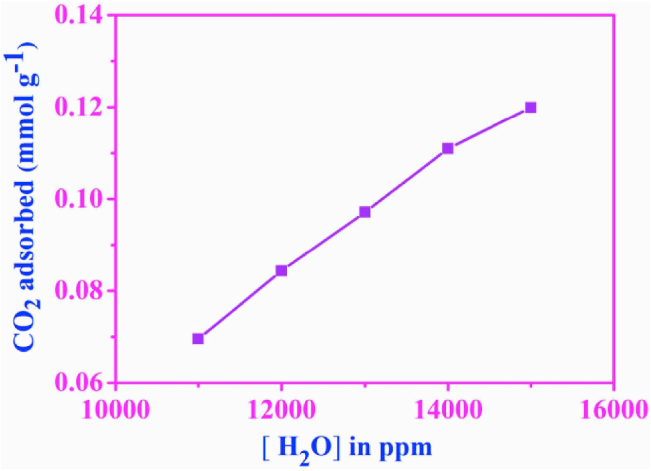

Fig. 27. Moisture dependent CO_2 trapping from the seasonal ambient air in clay based nanocomposites, reproduced with permission from Ref. [159].

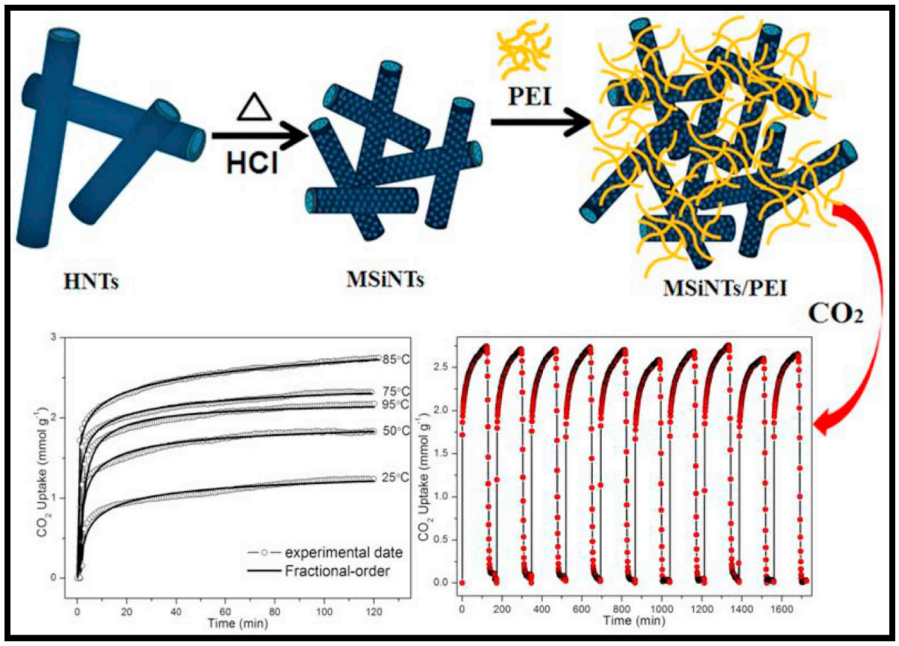

Fig. 28. Schematic presentation of the proposed synthesis of an emerging nanocomposite for CO_2 capture, taken from Ref. [161].

range of CO_2 pressures at a given temperature and at the excess sorption maximum, CO_2 sorption increases with decreasing temperature while the high pressure sorption properties demonstrate weak temperature dependence. Elliot A. Roth et al. [154] synthesized amine-containing solid sorbent for CO_2 capture through the modification of the surface of montmorillonite nanoclay using aminopropyltrimethoxysilane and polyethylenimine. They found that in pure CO_2 and 10% CO_2 in nitrogen gas streams the nanoclay loaded with only one of the amines exhibits $\sim$1.4 mmol g^{-1} capture efficacy, whereas it is $\sim$1.7 mmol g^{-1} CO_2 capture efficiency at 85 °C and atmospheric pressure when the nanoclay immobilized with both the amines. Xiao and co-workers [155] exploited an inexpensive and commercially available bentonite for CO_2 capture from flue gas after modified by sulfuric acid followed by immobilization of TEPA. H. T. Schaef et al. [156] reported the adsorption of CO_2 onto kaolinite surfaces under geologic sequestration conditions and verified through the density functional theory (DFT). A. G. Russell and co-workers utilized nanosepiolite as an inorganic-organic CO_2 sorbent (Fig. 26) by immobilizing tetraethylenepentamine (TEPA) onto acid-modified nanosepiolite, having capacity of 3 mmol g^{-1} for 1 vol % CO_2 in N_2, along with $\sim$1 vol % H_2O at 60 °C [157].

To demonstrate this aspect, Jana and co-workers [158] recently developed several HNTs based solid adsorbents being grafted with diverse aminosilanes containing both primary and/or secondary amine sites for CO_2 uptake from ambient air at 25 °C and ambient pressure. They were the first to explore the effect of relative humidity in terms of moisture on the adsorption kinetics by carrying out the experiment on the seasonal ambient air as shown in Fig. 27 [159]. This study demonstrates that relative humidity tunes the atmospheric CO_2 adsorption capacity of the adsorbents and corresponding adsorption kinetics. Authors also illustrated the adsorption kinetics of abundant isotopes of CO_2 ($^{12}C^{16}O_2$, $^{13}C^{16}O_2$, and $^{12}C^{16}O^{18}O$) present in the ambient air [160]. Tang and co-workers recently reported the fabrication of nanocomposites consisting of amine-impregnated mesoporous silica nanotube, synthesized through the impregnation of polyethenimine (PEI) onto mesoporous silica based nanonanotubes (HNTs) [161]. The nanocomposites loaded with PEI facilitate more CO_2 gas adsorption, having uptake capacity of 2.75 mmol g^{-1} at 85 °C for 2 h (Fig. 28). Authors also demonstrated that CO_2 adsorption on the nanocomposite occurs in a two-stage process; first, a sharp linear weight increase at the beginning and followed by a relatively slow adsorption step. They have also synthesized lithium orthosilicate (Li_4SiO_4)-based sorbents for high temperature CO_2 capture [162]. The sorbent was synthesized from HNTs through a solid-state reaction of lithium carbonate with acid treated HNTs in a Li: Si mixture with molar ratio of 4: 1 and then calcined at 800 °C for 4 h to produce Li_4SiO_4-based sorbents, having maximum CO_2 adsorption capacity of 7.8 mmol g^{-1}, and the temperature range of 350–720 °C. All these results suggest that these clay based low-cost adsorbents may introduce a new avenue in the frontier area of CO_2 capture and sequestration, which in turn make the procedure environmental friendly, robust, sustainable and an attractive strategy for CO_2 uptake.

3. Outlook and conclusions

In summary, we have demonstrated the prospect of CO_2 capture and critical analysis of several porous adsorbents for CO_2 capture and storage. We have discussed the developments of MOFs, ZIFs, POPs, COFs and mesoporous oxides for post-combustion CO_2 capture and illustrated the performance of these multifunctional porous solids towards adsorption and storage of CO_2. These adsorbents are usually judged in terms of their adsorption capacity but never put forward any effort to show how and why the adsorption and storage occurs. Consequently, a combination of structural, spectroscopic, thermodynamic experiments together with molecular simulation may provide answer to these entire questions, which are yet to be understood.

Unlike zeolites, the properties and functions of the pores can easily be tuned for specific applications as observed with these emerging MOFs, ZIFs, POPs and COFs, which in turn withdraw huge scientific demand as next-generation adsorbents for CO_2 removal. MOFs are beneficial with open porous networks and larger pores than zeolites, and thus favor self-diffusiveness or intra-crystalline diffusiveness during gas separation process. However, the thermal stability of MOFs is expected to be lower than that of zeolites/zeolite analogues because MOFs have lower metal-linker binding energy as compared to zeolites having stronger Si-O, Al-O linkages. Additionally, a number of aspects *e.g.*; stability, costs of preparation and regeneration after usage, energy input, large-scale synthesis etc. need to be carefully evaluated in addition to the adsorption capacity and selectivity before considering MOFs as an ideal sorbent for real application.

While we have enormous freedom for choosing ligands to construct

MOFs, ZIFs are merely restricted to imidazole derivatives in making hybrid microporous structure. Significantly, imidazoles having diverse polarities and symmetries can tune the CO_2 adsorption property of ZIFs without changing the transition metal cations, suggesting ZIFs have larger degree of freedom in building functional units than MOFs. Unlike MOFs, ZIFs have zeolite-like topology with better thermal and chemical stability, allowing them to work at wider temperature range. Another important aspect is that ZIFs are more hydrophobic than MOFs. ZIFs have identical efficiency in dry and humid condition with huge potential in selective CO_2 adsorption in moist condition, letting the adsorbent to store more carbon before reaching to the saturation, whereas MOFs would adsorb both water and CO_2, resulting in less storing capacity of carbon.

Although several progresses have been made for CO_2 adsorption in case of POPs, there are some issues still remaining: firstly, in order to solve the problem of scale-up economics, it is urgent to explore new synthesis conditions without noble metal catalysts; secondly, since CO_2 capture capacity at low pressure is more important than high pressure, POPs with multiple functional sites should be fabricated for better interaction with CO_2. Nevertheless, crystallinity of POPs is a major issue as amorphous POPs suffer from full accessibility towards CO_2 and it is also difficult to analyze their structural features which in turn restrict the understanding of their actual structure. Lastly, during CO_2 capture from flue gas, CO_2/N_2 and CO_2/CH_4 separation selectivity will not only be considered, but also need to overcome the difficulty of separation of other corrosive gases, like NO_x, SO_x, CO, O_2, and moisture. Therefore, POPs should be designed in such a way that they can come across these challenges.

COFs having high surface area and well crystalline frameworks, the diverse synthesis scope of functional COFs is lacking and they are incompetent as excellent CO_2 adsorbent compared to MOFs or POPs. Therefore, this issue should be addressed while designing the functional COFs with outstanding CO_2 storage property. On the contrary, mesoporous oxides and clays are an example of earth abundant materials and can be achieved in large scale, which in turn may open up a broader impact in using them as next-generation adsorbents. Although they possess high surface area, most of the functional groups are shrinked and embedded inside the pore wall owing to their layer structure and thus became inaccessible for CO_2 binding.

Consequently, we can say that CO_2 adsorption is a rising issue to combat with the exponential rise of world's population, leading to the increase in CO_2 concentration in atmosphere. Hence, mass production of efficient adsorbents is necessary to counter with the massive emission of CO_2. This issue can be well addressed from high-throughput screening of promising adsorbents viz., porous oxides and POPs which are mainly prepared from low-cost earth abundant elements. However, preparation of MOFs and ZIFs can't be ruled out from rare-earth elements and expensive linkers, whereas crystalline COFs are hardly prepared in large-scale through a convenient route. Thus, CO_2 adsorption is still an emerging field of research, which can bring forth significant progress in environmental and materials science by developing cost-effective adsorbents, introducing several possible routes in the frontier area of CO_2 capture and sequestration.

Conflicts of interest

The authors declare no competing financial interest.

Acknowledgement

This work was supported by SERB Women Excellence Award Grant (SB/WEA/08/2016) and Nano Mission Research Grant (SR/NM/NS-18/2014) funded by Department of Science and Technology (DST), Government of India. Authors also acknowledge the Technical Research Centre project (AI/1/64/SNB/2014) and S. N. Bose National Centre for Basic Sciences, Kolkata, India.

Abbreviations

HKUST	Hong Kong University of Science and Technology
IRMOF	IsoReticular Metal Organic Framework
MIL	Materials of Institut Lavoisier
BTC	1,3,5-benzene tricarboxylate
H_3BTB	1,3,5-tris(4-carboxyphenyl)-benzene
BDC	1,4-benzenedicarboxylate
UMCM-1	$[Zn_4O(BDC)(BTB)_{4/3}]$
DOT	2,5-dioxidoterephthalate
DOBC	2,5-dioxidobenzene-1,4-dicarboxylate
TATB	(4,4′,4″-*s*-triazine-2,4,6-triyl-tribenzoic acid)
H_3BTTri	1,3,5-tris(1H-1,2,3-triazol-5-yl)benzene
TMA	tetramethylammonium
TEA	tetraethylammonium
TBA	tetrabutylammonium
MER ZIF-60	$Zn_2(Im)_3(mIm)$
Im	imidazolate
mIm	2-methylimidazolate
GME-ZIF-68	Zn(bIm)(nIm)
bIm	benzimidazolate
nIm	Nitro imidazolate
LTA ZIF-20	$Zn(pur)_2$
DFT ZIF-3	$Zn_2(Im)_4$
RHO ZIF-11	$Zn(bIm)_2$
GIS ZIF-6	$Zn(Im)_2$
BTAP	benzothiazole polymers
$Ni(COD)_2$	Bis(1,5-cyclooctadiene)nickel(0)
DCE	Dichloroethane
PHAPs	Porous hyper-cross-linked aromatic polymers
PON	Polymeric organic network
HHTP	2,3,6,7,10,11–Hexahydroxytriphenylene
BTBA	1,3,5-benzenetriboronic acid
BTPB	1,3,5-tris[(4-phenylboronic acid]benzene
BPBA	4,4′-biphenyldiboronic acid
TBPM	tetra(4-dihydroxyborylphenyl)methane
TBPS	tetra(4-dihydroxyborylphenyl)silane
FPBA	4-formylphenylboronic acid
TAPB	1,3,5-tris(4-aminophenyl)-benzene
H_4abtc	1,1′-azobenzene-3,3′,5,5′-tetracarboxylic acid
Bdcppi	N,N′-bis(3,5-dicarboxyphenyl)pyromellitic diimide
BtetB	4,4′,4″,4‴-benzene-1,2,4,5-tetrayltetrabenzoic acid
diazDBC	3,3′,5,5′-azobenzenetetracarboxylic acid
p-CDC	1,12-dihydroxycarbonyl-1,12-dicarba-*closo*-dodecaborane
bpy	4,4′-bipyridine
bptb	2,2′-Penta(ethylene glycol)biphenyl-3,3′,5,5′- tetrakis(4 benzoic acid)
BdoborDC	1,12-Dicarba-closo-dodecaborane
mim	Methyl imidazole
TAPOP	triazatriangulenium
NOP	Nanoporous organic polymers
PECONFs	Porous electron-rich covalent organonitridic frameworks
13X	$5Na_2O.\ 5Al_2O_3.\ 14SiO_2.\ XH_2O$
WE-G 592	sodium aluminosilicates sodium form of type X crystal structure
APG-II	$Na_x[(AlO_2)_x.\ (SiO_2)_y].\ zH_2O$ – sodium form of type X molecular sieve
AP	3-Aminopropyl
DA	N-propylethylenediamine
TA	N-propyl diethylenetriamine
SM	Silica magenesium oxide composite
HT	hydrotalcite-like compounds
PEI	polyethyleneimine
M@RWY	Cation exchanged zeolitic chalcogenides
Mmen	N,N′-dimethylethylenediamine

References

[1] J. Hansen, R. Ruedy, M. Sato, K. Lo, Rev. Geophys. 48 (2010) RG4004.
[2] GISS Surface Temperature Analysis; http://data.giss.nasa.gov/gistemp/graphs_v3/(accessed January 2016).
[3] Q. Wang, J. Luo, Z. Zhong, A. Borgna, Energy Environ. Sci. 4 (2011) 42–55.
[4] D. Reichle, J. Houghton, B. Kane, J. Ekmann, Carbon Sequestration. State of the Science, U.S. Department of Energy, Office of Science, Office of Fossil Energy, Washington, DC, 1999.
[5] B.A. Oyenekan, G.T. Rochelle, AIChE J. 53 (2007) 3144–3154.
[6] B. Metz, O. Davidson, H.C. de Coninck, M. Loos, L.A. Meyer (Eds.), Special Report on Carbon Dioxide Capture and Storage. Prepared by Working Group III of the Intergovernmental Panel on Climate Change, Cambridge University Press, Cambridge, U.K. and New York, 2005.
[7] A. Demessence, D.M. D'Alessandro, M.L. Foo, J.R. Long, J. Am. Chem. Soc. 131 (2009) 8784–8786.
[8] N.P. Coutrin, V.J. Rose, A. Ouensanga, Fuel 84 (2005) 2131–2134.
[9] M. Steinberg, V.D. Dang, Energy Convers. 17 (1977) 97–112.
[10] E.S. Sanz-Pérez, C.R. Murdock, S.A. Didas, C.W. Jones, Chem. Rev. 116 (2016) 11840–11876.
[11] L. Czepirski, J. JagieŁŁo, Chem. Eng. Sci. 44 (1989) 797–801.
[12] H.H. Pan, J.A. Ritter, P.B. Balbuena, Langmuir 14 (1998) 6323–6327.
[13] J. Yu, L.H. Xie, J.R. Li, Y. Ma, J.M. Seminario, P.B. Balbuena, Chem. Rev. 117 (2017) 9674–9754.
[14] A.L. Myers, J.M. Prausnitz, AlChE J. 11 (1965) 121–127.
[15] Z.R. Herm, J.A. Swisher, B. Smit, R. Krishna, J.R. Long, J. Am. Chem. Soc. 133 (2011) 5664–5667.
[16] J. Gale, C. Hendriks, W. Turkenberg, A.H. Berger, A.S. Bhown, Energy Procedia 4 (2011) 562–567.
[17] H. He, W. Li, M. Zhong, D. Konkolewicz, D. Wu, K. Yaccato, T. Rappold, G. Sugar, N.E. David, K. Matyjaszewski, Energy Environ. Sci. 6 (2013) 488–493.
[18] X. Gao, B. Yu, Z. Yang, Y. Zhao, H. Zhang, L. Hao, B. Han, Z. Liu, ACS Catal. 5 (2015) 6648–6652.
[19] S.K. Wirawan, D. Creaser, Microporous Mesoporous Mater. 91 (2006) 196–205.
[20] K.T. Chue, J.N. Kim, Y.J. Yoo, S.H. Cho, R.T. Yang, Ind. Eng. Chem. Res. 34 (1995) 591–598.
[21] K. Sumida, D.L. Rogow, J.A. Mason, T.M. McDonald, E.D. Bloch, Z.R. Herm, T.H.T.H. Bae, J.R. Long, Chem. Rev. 112 (2012) 724–781.
[22] Y. Zeng, R. Zou, Y. Zhao, Adv. Mater. 28 (2016) 2855–2873.
[23] R. Dawson, D.J. Adams, A.I. Cooper, Chem. Sci. 2 (2011) 1173–1177.
[24] N. Mengya, Y. Huaming, Z. Xiangchao, W. Yutang, T. Aidong, ACS Appl. Mater. Interfaces 8 (2016) 17312–17320.
[25] M.S. Walters, T.F. Edgar, G.T. Rochelle, Ind. Eng. Chem. Res. 55 (2016) 4646–4657.
[26] T.G. Glover, G.W. Peterson, B.J. Schindler, D. Britt, O.M. Yaghi, Chem. Eng. Sci. 66 (2011) 163–170.
[27] M. Eddaoudi, J. Kim, N. Rosi, D. Vodak, J. Wachter, M. O'Keeffe, O.M. Yaghi, Science 295 (2002) 469–472.
[28] D. Farrusseng, C. Daniel, C. Gaudillère, U. Ravon, Y. Schuurman, C. Mirodatos, D. Dubbeldam, H. Frost, R.Q. Snurr, Langmuir 25 (2009) 7383–7388.
[29] B. Arstad, H. Fjellvag, K.O. Kongshaug, O. Swang, R. Blom, Adsorption 14 (2008) 755.
[30] A.R. Millward, O.M. Yaghi, J. Am. Chem. Soc. 127 (2005) 17998–17999.
[31] S. Bourrelly, P.L. Llewellyn, C. Serre, F. Millange, T. Loiseau, G. Férey, J. Am. Chem. Soc. 127 (2005) 13519–13521.
[32] P.J. Hagrman, D. Hagrman, J. Zubieta, Angew. Chem. Int. Ed. 38 (1999) 2638–2684.
[33] S.R. Batten, R. Robson, Angew. Chem. Int. Ed. 37 (1998) 1460–1494.
[34] H.C. Zhou, S. Kitagawa, Chem. Soc. Rev. 43 (2014) 5415–5418.
[35] C.A. Trickett, A. Helal, B.A. Al-Maythalony, Z.H. Yamani, K.E. Cordova, O.M. Yaghi, Nat. Rev. Mater. 2 (2017) 17045.
[36] D.M. D'Alessandro, B. Smit, J.F. Long, Angew. Chem. Int. Ed. 49 (2010) 6058–6082.
[37] N. Getachew, Y. Chebude, I. Diaz, M. Sanchez-Sanchez, J. Porous Mater. 21 (2014) 769–773.
[38] H. Li, M. Eddaoudi, M. O'Keeffe, O.M. Yaghi, Nature 402 (1999) 276–279.
[39] H. Furukawa, N. Ko, Y.B. Go, N. Aratani, S.B. Choi, E. Choi, Science 329 (2010) 424–428.
[40] D. Britt, H. Furukawa, B. Wang, T.G. Glover, O.M. Yaghi, Proc. Natl. Acad. Sci. U.S.A. 106 (2009) 20637–20640.
[41] K. Koh, A. Wong-Foy, A. Matzger, Angew. Chem. Int. Ed. 47 (2008) 677–680.
[42] O.S. Jung, Y.J. Kim, Y.A. Lee, J.K. Park, H.K. Chae, J. Am. Chem. Soc. 122 (2000) 9921–9925.
[43] K. Uemura, S. Kitagawa, K. Fukui, K. Saito, J. Am. Chem. Soc. 126 (2004) 3817–3828.
[44] A.O. Yazaydın, A.I. Benin, S.A. Faheem, P. Jakubczak, J.J. Low, R.R. Willis, R.Q. Snurr, Chem. Mater. 21 (2009) 1425–1430.
[45] S. Bourrelly, P.L. Llewellyn, C. Serre, F. Millange, T. Loiseau, G. Ferey, J. Am. Chem. Soc. 127 (2005) 13519–13521.
[46] A.C. Kizzie, A.G. Wong-Foy, A.J. Matzger, Langmuir 27 (2011) 6368–6373.
[47] J. Liu, P.K. Thallapally, B.P. McGrail, D.R. Brown, Chem. Soc. Rev. 41 (2012) 2308–2322.
[48] P.K. Thallapally, J. Tian, M.R. Kishan, C.A. Fernandez, S.J. Dalgarno, P.B. McGrail, J.E. Warren, J.L. Atwood, J. Am. Chem. Soc. 130 (2008) 16842–16843.
[49] K.S. Lin, A.K. Adhikari, C.N. Ku, C.L. Chiang, H. Kuo, Int. J. Hydrogen Energy 37 (2012) 13865–13871.
[50] H. Huang, W. Zhang, D. Liu, C. Zhong, Ind. Eng. Chem. Res. 51 (2012) 10031–10038.
[51] J.J. Low, A.I. Benin, P. Jakubczak, J.F. Abrahamian, S.A. Faheem, R.R. Willis, J. Am. Chem. Soc. 131 (2009) 15834–15842.
[52] S. Keskin, D.S. Sholl, Langmuir 25 (2009) 11786–11795.
[53] Y.E. Cheon, J. Park, M.P. Suh, Chem. Commun. (2009) 5436–5438.
[54] J. Kim, S.T. Yang, S.B. Choi, J. Sim, W.S. Ahn, J. Mater. Chem. 21 (2011) 3070–3076.
[55] J.L.C. Rowsell, O.M. Yaghi, J. Am. Chem. Soc. 128 (2006) 1304–1315.
[56] R. Babarao, J.W. Jiang, S.I. Sandler, Langmuir 25 (2009) 5239–5247.
[57] J.A. Botas, G. Calleja, M. Sanchez-Sanchez, M.G. Orcajo, Langmuir 26 (2010) 5300–5303.
[58] Y.S. Bae, O.K. Farha, J.T. Hupp, R.Q. Snurr, J. Mater. Chem. 19 (2009) 2131–2134.
[59] N.A. Ramsahye, G. Maurin, S. Bourrelly, P.L. Llewellyn, T. Devic, C. Serre, T. Loiseau, G. Ferey, Adsorption 13 (2007) 461–467.
[60] A. Vimont, A. Travert, P. Bazin, J.C. Lavalley, M. Daturi, C. Serre, G. Ferey, S. Bourrelly, P.L. Llewellyn, Chem. Commun. (2007) 3291–3293.
[61] R. Vaidhyanathan, S.S. Iremonger, K.W. Dawson, G.K.H. Shimizu, Chem. Commun. (2009) 5230–5232.
[62] A. Demessence, D.M. D'Alessandro, M.L. Foo, J.R. Long, J. Am. Chem. Soc. 131 (2009) 8784–8786.
[63] Z.Q. Wang, S.M. Cohen, J. Am. Chem. Soc. 131 (2009) 16675–16677.
[64] J. An, S.J. Geib, N.L. Rosi, J. Am. Chem. Soc. 132 (2010) 38–39.
[65] R. Banerjee, A. Phan, B. Wang, C. Knobler, H. Furukawa, M. O'Keeffe, O.M. Yaghi, Science 319 (2008) 939–943.
[66] N.T.T. Nguyen, T.N.H. Lo, J. Kim, H.T.D. Nguyen, T.B. Le, K.E. Cordova, H. Furukawa, Inorg. Chem. 55 (2016) 6201–6207.
[67] J. An, N.L. Rosi, J. Am. Chem. Soc. 132 (2010) 5578–5579.
[68] Y.Q. Tian, Z.X. Chen, L.H. Weng, H.B. Guo, S. Gao, D.Y. Zhao, Inorg. Chem. 43 (2004) 4631–4635.
[69] S.A. Moggach, T.D. Bennett, A.K. Cheetham, Angew. Chem. Int. Ed. 121 (2009) 7221–7223.
[70] A. Phan, C.J. Doonan, F.J. Uribe-Romo, C.B. Knobler, M. O'Keeffe, O.M. Yaghi, Acc. Chem. Res. 43 (2010) 58–67.
[71] D. Bradshaw, A. Garai, J. Huo, Chem. Soc. Rev. 41 (2012) 2344–2381.
[72] M. Zhou, Q. Wang, L. Zhang, Y.C. Liu, Y. Kang, J. Phys. Chem. B 113 (2009) 11049–11053.
[73] C. Chen, J. Kim, D.A. Yang, W.S. Ahn, Chem. Eng. J. 168 (2011) 1134–1139.
[74] W. Morris, N. He, K.G. Ray, P. Klonowski, H. Furukawa, I.N. Daniels, Y.A. Houndonougbo, M. Asta, O.M. Yaghi, B.B. Laird, J. Phys. Chem. C 116 (2012) 24084–24090.
[75] P. Küsgens, M. Rose, I. Senkovska, H. Froede, A. Henschel, S. Siegle, S. Kaskel, Microporous Mesoporous Mater. 120 (2009) 325–330.
[76] A.U. Ortiz, A.P. Freitas, A. Boutin, A.H. Fuchs, F.X. Coudert, Phys. Chem. Chem. Phys. 16 (2014) 9940–9949.
[77] E.V.R. Fernandez, A.G. Atienza, D. Farrusseng, S. Aguado, J. Mater. Chem. A 6 (2018) 5598–5602.
[78] Q. Song, S. Nataraj, M. V Roussenova, J. C Tan, D. J Hughes, W. Li, P. Bourgoin, M.A. Alam, A. K Cheetham, S.A. Al-Muhtaseb, E. Sivaniah, Energy Environ. Sci. 5 (2012) 8359–8369.
[79] E. Shamsaei, X. Lin, Z.X. Low, Z. Abbasi, Y. Hu, J.Z. Liu, H. Wang, ACS Appl. Mater. Interfaces 8 (2016) 6236–6244.
[80] Z. Zhang, S. Xian, Q. Xia, H. Wang, Z. Li, J. Li, AIChE J. 59 (2013) 2195–2206.
[81] D. Liu, Y. Wu, Q. Xia, Z. Li, H. Xi, Adsorption 19 (2013) 25–37.
[82] F. Gao, Y. Li, Z. Bian, J. Hu, H. Liu, J. Mater. Chem. A 3 (2015) 8091–8097.
[83] Y. He, X. Zhu, Y. Li, C. Peng, J. Hu, H. Liu, Microporous Mesoporous Mater. 214 (2015) 181–187.
[84] A. Modak, J. Mondal, A. Bhaumik, ChemCatChem 5 (2013) 1749–1753.
[85] A. Modak, A. Bhaumik, ChemistrySelect 6 (2016) 1192–1200.
[86] Y. Xu, S. Jin, H. Xu, A. Nagai, D. Jiang, Chem. Soc. Rev. 42 (2013) 8012–8031.
[87] S. Das, P. Heasman, T. Ben, S. Qiu, Chem. Rev. 117 (2017) 1515–1563.
[88] L. Zou, Y. Sun, S. Che, X. Yang, X. Wang, M. Bosch, Q. Wang, H. Li, M. Smith, S. Yuan, Z. Perry, H.C. Zhou, Adv. Mater. 29 (2017) 1700229–1700264.
[89] X. Feng, X.S. Ding, D.L. Jiang, Chem. Soc. Rev. 41 (2012) 6010–6022.
[90] X.F. Jing, D.L. Zou, P. Cui, H. Ren, G.S. Zhu, J. Mater. Chem.A 1 (2013) 13926–13931.
[91] Z. Yang, X. Peng, D. Cao, J. Phys. Chem. C 117 (2013) 8353–8364.
[92] N. Chaoui, M. Trunk, R. Dawson, J. Schmidt, A. Thomas, Chem. Soc. Rev. 46 (2017) 3302–3321.
[93] X. Zhu, C. Tian, S.M. Mahurin, S.H. Chai, C. Wang, S. Brown, G.M. Veith, H. Luo, H. Liu, S. Dai, J. Am. Chem. Soc. 134 (2012) 10478–10484.
[94] Z.H. Guo, C. Wang, Q. Zhang, S. Che, H.C. Zhou, L. Fang, Mater. Chem. Front. 2 (2018) 396–401.
[95] S.H. Je, O. Buyukcakir, D. Kim, A. Coskun, Inside Chem. 1 (2016) 482–493.
[96] O. Buyukcakir, S.H. Je, J. Park, H.A. Patel, Y. Jung, C.T. Yavuz, A. Coskun, Chem. Eur J. 21 (2015) 15320–15327.
[97] T. Ben, H. Ren, S. Ma, D. Cao, J. Lan, X. Jing, W. Wang, J. Xu, F. Deng, J.M. Simmons, S. Qiu, G. Zhu, Angew. Chem. Int. Ed. 48 (2009) 9457–9460.
[98] D. Yuan, W. Lu, D. Zhao, H.C. Zhou, Adv. Mater. 23 (2011) 3723–3725.
[99] L. Tan, B. Tan, Chem. Soc. Rev. 46 (2017) 3322–3356.
[100] R. Dawson, L.A. Stevens, T.C. Drage, C.E. Snape, M.W. Smith, D.J. Adams, A.I. Cooper, J. Am. Chem. Soc. 134 (2012) 10741–10744.
[101] A. Modak, Y. Maegawa, Y. Goto, S. Inagaki, Polym. Chem. 7 (2016) 1290–1296.
[102] P. Puthiaraj, W.S. Ahn, Ind. Eng. Chem. Res. 55 (2016) 7917–7923.

[103] S.H. Jia, X. Ding, H. T Yu, B.H. Han, RSC Adv. 5 (2015) 71095–71101.
[104] H.J. Jeon, J.H. Choi, Y. Lee, K.M. Choi, J.H. Park, J.K. Kang, Adv. Energy Mater. 2 (2012) 225–228.
[105] Q. Chen, M. Luo, P. Hammershoj, D. Zhou, Y. Han, B.W. Laursen, C.G. Yan, B.H. Han, J. Am. Chem. Soc. 134 (2012) 6084–6087.
[106] Q. Chen, D.P. Liu, M. Luo, L.J. Feng, Y.C. Zhao, B.H. Han, Small 10 (2014) 308–315.
[107] X. Zhu, C. Tian, S.M. Mahurin, S.H. Chai, C. Wang, S. Brown, G.M. Veith, H. Luo, H. Liu, S. Dai, J. Am. Chem. Soc. 134 (2012) 10478–10484.
[108] S. Nandi, U. Werner-Zwanziger, R. Vaidhyanathan, J. Mater. Chem. A 3 (2015) 21116–21122.
[109] P. Katekomol, J. Roeser, M. Bojdys, J. Weber, A. Thomas, Chem. Mater. 25 (2013) 1542–1548.
[110] C. Gu, D. Liu, W. Huang, J. Liu, R. Yang, Polym. Chem. 6 (2015) 7410–7417.
[111] K. Wang, H. Huang, D. Liu, C. Wang, J. Li, C. Zhong, Environ. Sci. Technol. 50 (2016) 4869–4876.
[112] S. Ren, R. Dawson, A. Laybourn, J.-x. Jiang, Y. Khimyak, D.J. Adams, A.I. Cooper, Polym. Chem. 3 (2012) 928–934.
[113] L. Meng, X. Zou, S. Guo, H. Ma, Y. Zhao, G. Zhu, ACS Appl. Mater. Interfaces 7 (2015) 15561–15569.
[114] Z. Wang, S. Yuan, A. Mason, B. Reprogle, D.J. Liu, L. Yu, Macromolecules 45 (2012) 7413–7419.
[115] N. U Day, C. Wamser, M.G. Walter, Polym. Int. 64 (2015) 833–857.
[116] A. Modak, M. Nandi, J. Mondal, A. Bhaumik, Chem. Commun. 48 (2012) 248–250.
[117] A. Modak, M. Pramanik, S. Inagaki, A. Bhaumik, J. Mater. Chem. A 2 (2014) 11642–11650.
[118] H.A. Patel, J.S.H. Park, D.P. Chen, Y. Jung, C.T. Yavuz, A. Coskun, Nat. Commun. 4 (2013) 1357.
[119] P. Arab, M.G. Rabbani, A.K. Sekizkardes, T. İslamoğlu, H.M. El-Kaderi, Chem. Mater. 26 (2014) 1385–1392.
[120] J.R. Holst, E. Stockel, D.J. Adams, A.I. Cooper, Macromolecules 43 (2010) 8531–8538.
[121] W. Fan, X. Liu, Z. Zhang, Q. Zhang, W. Ma, D. Tan, A. Li, Microporous Mesoporous Mater. 196 (2014) 335–340.
[122] J.H. Ko, N. Kang, N. Park, H.W. Shin, S. Kang, S.M. Lee, H.J. Kim, T.K. Ahn, S.U. Son, ACS Macro Lett. 4 (2015) 669–672.
[123] X. Feng, Y. Liang, L. Zhi, A. Thomas, D. Wu, I. Lieberwirth, U. Kolb, K. Mullen, Adv. Funct. Mater. 19 (2009) 2125–2129.
[124] Y. Chen, H. Sun, R. Yang, T. Wang, C. Pei, Z. Xiang, Z. Zhu, W. Liang, A. Li, W. Deng, J. Mater. Chem. A 3 (2015) 87–91.
[125] S.K. Das, X. Wang, M.M. Ostwal, Y. Zhao, Y. Han, Z. Lai, Chem. Eng. Sci. 145 (2016) 21–30.
[126] A. Sharma, A. Malani, N.V. Medhekar, R. Babarao, CrystEngComm 19 (2017) 6950–6963.
[127] A.P. Cote, A.I. Benin, N.W. Ockwig, M. O'Keeffe, A.J. Matzger, O.M. Yaghi, Science 310 (2005) 1166–1170.
[128] H. Furukawa, O.M. Yaghi, J. Am. Chem. Soc. 131 (2009) 8875–8883.
[129] R.W. Tilford, W.R. Gemmill, H.C. Loye, J.J. Lavigne, Chem. Mater. 18 (2006) 5296–5301.
[130] H.M. El-Kaderi, J.R. Hunt, J.L. Mendoza-Cortes, A.P. Cote, R.E. Taylor, M. O'Keeffe, O.M. Yaghi, Science 316 (2007) 268–272.
[131] R. Babarao, J. Jiang, Energy Environ. Sci. 1 (2008) 139–143.
[132] Z. Kahveci, T. Islamoglu, G.A. Shar, R. Ding, H.M. El-Kaderi, CrystEngComm 15 (2013) 1524–1527.
[133] F.J. Uribe-Romo, J.R. Hunt, H. Furukawa, C. Klock, M. O'Keeffe, O.M. Yaghi, J. Am. Chem. Soc. 131 (2009) 4570–4571.
[134] F.J. Uribe-Romo, C.J. Doonan, H. Furukawa, K. Oisaki, O.M. Yaghi, J. Am. Chem. Soc. 133 (2011) 11478–11481.
[135] S. Kandambeth, A. Mallick, B. Lukose, M.V. Mane, T. Heine, R. Banerjee, J. Am. Chem. Soc. 134 (2012) 19524–19527.
[136] A. Modak, J. Mondal, V.K. Aswal, A. Bhaumik, J. Mater. Chem. 20 (2010) 8099-8016.
[137] A. Modak, M. Nandi, A. Bhaumik. Catal. Today 198 (2012) 45–51.
[138] A. Modak, J. Mondal, A. Bhaumik, Green Chem. 14 (2012) 2840–2855.
[139] B.P. Biswal, S. Chandra, S. Kandambeth, B. Lukose, T. Heine, R. Banerjee, J. Am. Chem. Soc. 135 (2013) 5328–5331.
[140] S. Kandambeth, D.B. Shinde, M.K. Panda, B. Lukose, T. Heine, R. Banerjee, Angew. Chem. Int. Ed. 52 (2013) 13052–13056.
[141] Y. Du, D. Calabro, B. Wooler, P. Kortunov, Q.C. Li, S. Cundy, K.M. Mao, Chem. Mater. 27 (2015) 1445–1447.
[142] M.G. Rabbani, A.K. Sekizkardes, Z. Kahveci, T.E. Reich, R. Ding, H.M. El-Kaderi, Chem. Eur J. 19 (2013) 3324–3328.
[143] F.J.U. Romo, C.J. Doonan, H. Furukawa, K. Oisaki, O.M. Yaghi, J. Am. Chem. Soc. 133 (2011) 11478–11481.
[144] Y. Zeng, R. Zou, Z. Luo, H. Zhang, X. Yao, X. Ma, R. Zou, Y. Zhao, J. Am. Chem. Soc. 137 (2015) 1020–1023.
[145] N. Huang, R. Krishna, D. Jiang, J. Am. Chem. Soc. 137 (2015) 7079–7082.
[146] R.M. Myers, D.E. Fitzpatrick, R.M. Turner, S.V. Ley, Chem. Eur J. 20 (2014) 12348–12366.
[147] S. Wan, J. Guo, J. Kim, H. Ihee, D. Jiang, Angew. Chem. 120 (2008) 8958–8962.
[148] R. Kishor, A.K. Ghoshal, Ind. Eng. Chem. Res. 56 (2017) 6078–6087.
[149] L.A. Darunte, A.D. Oetomo, K.S. Walton, D.S. Sholl, C.W. Jones, ACS Sustain. Chem. Eng. 4 (2016) 5761–5768.
[150] M. Caplow, J. Am. Chem. Soc. 90 (1968) 6795–6803.
[151] P.V. Danckwerts, Chem. Eng. Sci. 34 (1979) 443–446.
[152] W. Wang, J. Xiao, X. Wei, J. Ding, X. Wang, C. Song, Appl. Energy 113 (2014) 334–341.
[153] G. Rother, E.S. Ilton, D. Wallacher, T. Hau, H.T. Schaef, O. Qafoku, K.M. Rosso, A.R. Felmy, E.G. Krukowski, A.G. Stack, N. Grimm, R.J. Bodnar, Environ. Sci. Technol. 47 (2013) 205–211.
[154] E.A. Roth, S. Agarwal, R.K. Gupta, Energy Fuels 27 (2013) 4129–4136.
[155] W. Wang, X. Wang, C. Song, X. Wei, J. Ding, J. Xiao, Energy Fuels 27 (2013) 1538–1546.
[156] H.T. Schaef, V.A. Glezakou, A.T. Owen, S. Ramprasad, P.F. Martin, B.P. McGrail, Environ. Sci. Technol. Lett. 1 (2014) 142–145.
[157] M. Irani, M. Fan, H. Ismail, A. Tuwati, B. Dutcher, A.G. Russell, Nanomater. Energy 11 (2015) 235–246.
[158] S. Das, A. Maity, M. Pradhan, S. Jana, Anal. Chem. 88 (2016) 2205–2211.
[159] S. Das, C. Ghosh, S. Jana, J. Mater. Chem. A 4 (2016) 7632–7640.
[160] S. Jana, S. Das, C. Ghosh, A. Maity, M. Pradhan, Sci. Rep. 5 (2015) 8711.
[161] M. Niu, H. Yang, X. Zhang, Y. Wang, A. Tang, ACS Appl. Mater. Interfaces 8 (2016) 17312–17320.
[162] M. Niu, X. Li, J. Ouyang, H. Yang, RSC Adv. 6 (2016) 44106–44112.
[163] Y.G. Lee, H.R. Moon, Y.E. Cheon, M.P. Suh, Angew. Chem. Int. Ed. 47 (2008) 7741–7745.
[164] T.K. Prasad, D.H. Hong, M.P. Suh, Chem. Eur J. 16 (2010) 14043–14050.
[165] X. Guo, G. Zhu, Z. Li, F. Sun, Z. Yang, S. Qiu, Chem. Commun. (2006) 3172–3174.
[166] X. Si, C. Jiao, F. Li, J. Zhang, S. Wang, S. Liu, Z. Li, L. Sun, F. Xu, Z. Gabelica, C. Schick, Energy Environ. Sci. 4 (2011) 4522–4527.
[167] Q. Yan, Y. Lin, C. Kong, L. Chen, Chem. Commun. 49 (2013) 6873–6875.
[168] Y.S. Bae, O.K. Farha, J.T. Hupp, R.Q. Snurr, J. Mater. Chem. 19 (2009) 2131–2134.
[169] J. Moellmer, E.B. Celer, R. Luebke, A.J. Cairns, R. Staudt, M. Eddaoudi, M. Thommes, Microporous Mesoporous Mater. 129 (2010) 345–353.
[170] T.M. McDonald, D.M. D'Alessandro, R. Krishna, J.R. Long, Chem. Sci. 2 (2011) 2022–2028.
[171] O.K. Farha, A.M. Spokoyny, K.L. Mulfort, S. Galli, J.T. Hupp, C.A. Mirkin, Small 15 (2009) 1727–1731.
[172] A. Kondo, A. Chinen, H. Kajiro, T. Nakagawa, K. Kato, M. Takata, Y. Hattori, F. Okino, T. Ohba, K. Kaneko, H. Kanoh, Chem. Eur J. 15 (2009) 7549–7553.
[173] S. Wu, L. Ma, L.S. Long, L.S. Zheng, W. Lin, Inorg. Chem. 48 (2009) 2436–2442.
[174] A.M. Spokoyny, O.K. Farha, K.L. Mulfort, J.T. Hupp, C.A. Mirkin, Inorg. Chim. Acta. 364 (2010) 266–271.
[175] A.J. Fletcher, E.J. Cussen, D. Bradshaw, M.J. Rosseinsky, K.M. Thomas, J. Am. Chem. Soc. 126 (2004) 9750–9759.
[176] Y.Q. Tian, S.Y. Yao, D. Gu, K.H. Cui, D. W, G. Zhang, Z.X. Chen, D.Y. Zhao, Chem. Eur J. 16 (2010) 1137–1141.
[177] J. Moellmer, A. Moeller, F. Dreisbach, R. Glaeser, R. Staudt, Microporous Mesoporous Mater. 138 (2011) 140–148.
[178] Q.M. Wang, D. Shen, M. Bulow, M.L. Lang, S. Deng, F.R. Fitch, N.O. Lemcoff, J. Semanscin, Microporous Mesoporous Mater. 55 (2002) 217–230.
[179] Z. Liang, M. Marshall, A.L. Chaffee, Energy Fuels 23 (2009) 2785–2789.
[180] L. Hamon, E. Jolimaitre, G.D. Pirngruber, Ind. Eng. Chem. Res. 49 (2010) 7497–7503.
[181] E.V. Perez, K.J. Balkus, J.P. Ferraris, I.H. Musselman, J. Membr. Sci. 328 (2009) 165–173.
[182] Z. Zhao, Z. Li, Y.S. Lin, Ind. Eng. Chem. Res. 48 (2009) 10015–10020.
[183] Q. Xu, D.H. Liu, Q.Y. Yang, C.L. Zhong, J.G. Mi, J. Mater. Chem. 20 (2010) 706–714.
[184] P.S. Bárcia, L. Bastin, E.J. Hurtado, J.A.C. Silva, A.E. Rodrigues, B. Chen, Separ. Sci. Technol. 43 (2008) 3494–3521.
[185] P.L. Llewellyn, S. Bourrelly, C. Serre, A. Vimont, M. Daturi, L. Hamon, G.D. Weireld, J.S. Chang, D.Y. Hong, Y.K. Hwang, S.H. Jhung, G. Férey, Langmuir 24 (24) (2008) 7245–7250.
[186] J. An, N.L. Rosi, J. Am. Chem. Soc. 132 (2010) 5578–5579 132.
[187] J. Perez-Pellitero, H. Amrouche, F.R. Siperstein, G. Pirngruber, C. Nieto-Draghi, G. Chaplais, A. Simon-Masseron, D. Bazer-Bachi, D. Peralta, N. Bats, Chem. Eur J. 16 (2010) 1560–1561.
[188] M.J. C Ordoñez, K.J. J Balkus, J.P. Ferraris, I.H.J. Musselman, Membr. Sci. 361 (2010) 28–37.
[189] X.M. Hu, Q. Chen, Z.Y. Sui, Z.Q. Zhao, N. Bovet, B.W. Laursen, B.H. Han, RSC Adv. 5 (2015) 90135–90143.
[190] D. Chen, S. Gu, Y. Fu, Y. Zhu, C. Liu, G. Li, G. Yu, C. Pan, Polym. Chem. 7 (2016) 3416–3422.
[191] P. Mohanty, L.D. Kull, K. Landskron, Nat. Commun. 2 (2011) 401.
[192] R. Yuan, H. Ren, Z. Yan, A. Wang, G. Zhu, Polym. Chem. 5 (2014) 2266–2272.
[193] W. Lu, D. Yuan, J. Sculley, D. Zhao, R. Krishna, H.C. Zhou, J. Am. Chem. Soc. 133 (2011) 18126–18129.
[194] W. Lu, W.M. Verdegaal, J. Yu, P.B. Balbuena, H.K. Jeong, H.C. Zhou, Energy Environ. Sci. 6 (2013) 3559–3564.
[195] H. Ma, H. Ren, X. Zou, S. Meng, F. Sun, G. Zhu, Polym. Chem. 5 (2014) 144–152.
[196] R. Gomes, P. Bhanja, A. Bhaumik, Chem. Commun. 51 (2015) 10050–10053.

[197] S. Chandra, S. Kandambeth, B.P. Biswal, B. Lukose, S.M. Kunjir, M. Chaudhary, R. Babarao, T. Heine, R. Banerjee, J. Am. Chem. Soc. 135 (2013) 17853–17861.
[198] Y. Zhao, K.X. Yao, B. Teng, T. Zhang, Y. Han, Energy Environ. Sci. 6 (2013) 3684–3692.
[199] Z. Li, Y. Zhi, X. Feng, X. Ding, Y. Zou, X. Liu, Y. Mu, Chem. Eur J. 21 (2015) 12079–12084.
[200] Z. Li, X. Feng, Y. Zou, Y. Zhang, H. Xia, X. Liu, Y. Mu, Chem. Commun. 50 (2014) 13825–13828.
[201] C. Chen, W.S. Ahn, Chem. Eng. J. 166 (2011) 646.
[202] M.G. Plaza, C. Pevida, B. Arias, J. Fermoso, A. Arenillas, F. Rubiera, J.J. Pis, J. Therm. Anal. Calorim. 92 (2008) 601.
[203] V. Zeleňák, M. Skřínska1, A. Zukal, J. Čejka, Chem. Eng. J. 348 (2018) 327–333.
[204] G. Song, X. Zhu, R. Chen, Q. Liao, Y.D. Ding, L. Chen, Chem. Eng. J. 283 (2016) 175–183.
[205] C. Gunathilake, Mietek Jaroniec, J. Mater. Chem. A 4 (2016) 10914–10924.
[206] M. Bhagiyalakshmi, J.Y. Lee, H.T. Jang, Int. J. Greenhouse Gas Control 4 (2010) 51–56.
[207] X. Wang, J.J. Yu, J. Cheng, Z.P. Hao, Z.P. Xu, Environ. Sci. Technol. 42 (2008) 614–618.
[208] B. Ficicilar, T. Dogu, Catal. Today 115 (2006) 274–278.
[209] L. Mafra, T. Čendak, S. Schneider, P.V. Wiper, J. Pires, J.R.B. Gomes, M.L. Pinto, Chem. Eng. J. 336 (2018) 612–621.
[210] Q. Liu, N.C.O. Cheung, A.E. Garcia-Bennett, N. Hedin, ChemSusChem 4 (2011) 91–97.
[211] R.V. Siriwardane, M.S. Shen, E.P. Fisher, Energy Fuels 19 (2005) 1153–1159.
[212] M. Mofarahi, F. Gholipour, Microporous Mesoporous Mater. 200 (2014) 1–10.
[213] M.H. Zarghampoor, M. Mozaffarian, M. Soleimani, M.T. Ravanchi, IOP Conf. Ser. Mater. Sci. Eng. 206 (2017) 012004.
[214] C. Chen, J. Kim, W.S. Ahn, Kor. J. Chem. Eng. 31 (2014) 1919–1934.
[215] S. Kumar, K. Prasad, J.M. Gil, A.J.F.N. Sobral, J. Koh, Carbohydr. Polym. 198 (2018) 401–406.
[216] H. Yang, M. Luo, X. Chen, X. Zhao, § J. Lin, D. Hu, D. Li, X. Bu, P. Feng, T. Wu, Inorg. Chem. 56 (2017) 14999–15005.

Arindam Modak is currently working as Scientist C in Technical Research Centre Project of S. N. Bose National Centre for Basic Sciences, India. He received his PhD degree in materials science from Indian Association for the Cultivation of Science (IACS), India. Prior to joining in S. N. Bose Centre, he was a post doctoral associate in Toyota Central R & D Labs. INC., Japan. His research focuses on the development of functional organic and organic-inorganic hybrid porous materials as adsorbent for CO_2 storage and conversion, along with utilizing them as solid catalyst for C-C bond formation, hydrogenation, biomass conversion, oxidation reactions etc. He is the recipient of prestigious CAS President's International Fellowship Initiative (PIFI) award on 2017 during his visit to China.

Subhra Jana received her Ph.D. in Chemistry from Indian Institute of Technology Kharagpur, India. She did her postdoctoral research work in the Department of Chemical Engineering, The Pennsylvania State University, USA. She is currently working as a DST INSPIRE Faculty at S. N. Bose National Centre for Basic Sciences, India. Her current research interests primarily focus on the syntheses and applications of metal-based nanostructured materials and hybrid nanocomposites in the field of heterogeneous catalysis and environmental remediation. Her work has been recognized by “Young Associate Award” from Indian Academy of Sciences, Bangalore and “SERB Women Excellence Award” from Department of Science & Technology (DST), India.